NJC

PAPER

Cite this: *New J. Chem.*, 2019, **43**, 19379

Impact of the donor substituent on the optoelectrochemical properties of 6*H*-indolo[2,3-*b*]quinoxaline amine derivatives†

Pooja S. Singh,‡ Purav M. Badani‡ and Rajesh M. Kamble *

Received 6th November 2019,
Accepted 13th November 2019

DOI: 10.1039/c9nj05558d

rsc.li/njc

A series of donor–acceptor-based 6*H*-indolo[2,3-*b*]quinoxaline amine derivatives were synthesized with different donor amines. The impact of the different donor moieties on 6*H*-indolo[2,3-*b*]quinoxaline was systematically examined by absorption-emission spectroscopy, cyclic voltammetry and theoretical studies. The photophysical properties of these molecules, such as intramolecular charge transfer transitions (400 to 462 nm) and emission (491 to 600 nm), were influenced by the nature of the peripheral amines. Further, the solid-state emission demonstrated by some of the dyes aroused our interest in performing photophysical studies on the aggregation-induced emission phenomenon; these dyes showed nanoparticle formation in THF/H_2O solvent mixtures. Varying the strength of the peripheral amines in the derivatives also tuned the electrochemical data, with lower band gaps (1.56 to 2.21 eV) and comparable HOMO–LUMO energy levels with reported ambipolar materials. The donor–acceptor architectures and HOMO–LUMO energies were further rationalized using DFT/TDDFT calculations. Thus, the opto-electrochemical studies and high thermal stability of these molecules indicate their potential application as solid-state emissive, ambipolar materials in optoelectronic devices.

Introduction

Indolo-quinoxalines are an important class of 'N'-containing heterocyclic compounds with inbuilt donor–acceptor (D–A) systems originating from their electron-rich indole units fused with the electron-deficient quinoxaline moiety. In addition to their fascinating biological applications[1] in the pharmaceutical industry, indolo-quinoxalines have been studied for application in optoelectronic devices[2] and as photo-initiators[3] due to their high thermal stability. The electronic properties of indolo-quinoxalines are sensitive towards the substituting position and strength of electron-donating groups along with the solvents used;[2a,4] the opto-electronic properties and thermal stability can be tuned by modifying the donor substituent in the D–A framework. Intended amalgamation of small D–A molecules with various electron donating or withdrawing substituents facilitates unique properties such as well-defined structures, ease of purification, solubility in a wide range of organic solvents, tuneable opto-electrochemical properties and greater thermal stability than polymeric materials.[5] In addition, the intramolecular charge transfer transition (ICT) characteristics of D–A systems containing electron-donating amines are mainly responsible for the tuning of their opto-electrochemical properties, leading to small band gap semiconducting materials.[6] As a result, proper selection of a D–A system helps obtain required luminescence and charge transporting properties in a molecule. Various D–A frameworks bearing electron-deficient/acceptor core compounds, such as quinoxaline,[7] indolo-quinoxaline,[2] and phenazine,[8] with electron-rich triarylamine/heterocyclic amines have been synthesized and explored for application in electroluminescence devices in the past.

The major shortcoming of amine-substituted D–A molecules is intermolecular stacking interactions caused by the presence of bulkier groups around the trigonal amine nitrogen, which are detrimental to the emission characteristics in the solid/aggregate state.[2a] As a result, most D–A molecules are emissive in dilute solutions but non-emissive or quenched in the aggregate/solid state, which leads to the aggregation-caused quenching (ACQ) effect due to a non-radiative relaxation process taking place inside the molecule.[9] However, for the practical application of these molecules in optoelectronic devices, mainly in OLEDs,[10] strong solid state emission is essential. Thus, in 2001, Tang *et al.* suggested a new idea, the aggregation-induced emission (AIE) phenomenon, in order to obtain solid state-emissive materials;

Department of Chemistry, University of Mumbai, Santacruz (E), Mumbai 400 098, India. E-mail: kamblerm@chem.mu.ac.in

† Electronic supplementary information (ESI) available: ^{1}H NMR, ^{13}C NMR, DEPT-135, FTIR and MALDI-TOF spectra of **1–9**; photophysical data, including UV-vis absorption spectra; fluorescence emission spectra and images; AIE and DLS spectra of **2**, **3**, **5**, **8** and **9**; cyclic voltammograms of **1–9**; and DFT and TDDFT calculation data along with optimized structures and molecular orbital diagrams are available in the ESI. See DOI: 10.1039/c9nj05558d

‡ Co-author.

AIE governs the ACQ effect by a strategy of restricted intramolecular rotation (RIR) and conformational changes in the molecules.[11] Thus, appropriate blending of AIE active groups with conventional ACQ blocks helps afford solid state emissive materials.[12]

Simultaneously, ambipolar materials deliver injection/transportation of both electrons and holes under ambient conditions, with a corresponding HOMO energy level of $\geq$5.6 eV and a LUMO level around 3.15 eV; this improves the recombination frequency of excitons.[7d,13] Thus, there is increased demand for electron transporting (n-type) and ambipolar materials compared to p-type materials for the development of high-efficiency and environmentally stable organic electronic devices. However, more p-type materials than n-type/ambipolar materials have been reported due to their difficult synthesis and instability of the latter under ambient conditions. However, hole transporting materials can be modulated into electron transporting materials by introducing electron withdrawing groups, such as carbonyl, cyano and perfluorinated alkyl chains, and a more electronegative atom than carbon in an extended p-system.[14] The redox process in small D–A molecules is based on transfer of charges from electron donating groups to electron withdrawing moieties within the system. Thus, fusion of an appropriate donor with an acceptor moiety within a molecule can aid the fabrication of ambipolar transporting materials.[15]

Considering the importance of indolo-quinoxaline, solid state emissive and ambipolar D–A materials, we have designed and synthesized amine derivatives **2–9** based on a 6*H*-indolo[2,3-*b*]quinoxaline segment by introducing various diarylamine/heterocyclic amines as donor units at the 2nd and 9th positions of **1** using Buchwald–Hartwig amination[16] reactions. The structures of dyes **2–9** are shown in Fig. 1. Most of the indolo-quinoxaline derivatives functionalized over the 8th or 9th position of the indole subunit reported to date have been studied for optoelectronic applications.[2] However, to the best of our knowledge, changes in the opto-electronic properties of indolo-quinoxaline molecules by substitution of amine groups at the quinoxaline segment or both sides have not been studied to date. Addition of electron-donating amine substituents to both the indole and quinoxaline nucleus may increase the push–pull interaction of the D–A framework between the indole and quinoxaline units. As a consequence, in this work, we attempted to study the changes occurring in the photophysical, electrochemical and thermal properties of **2–9** by incorporating different diaryl/heterocyclic amines as donor moieties on both the indole and quinoxaline segments. Further, the effects of substituting the diarylamines with electron donating ($-OCH_3$) and withdrawing ($-NO_2$, –N=N–Ph) groups on their opto-electrochemical properties, such as ICT, HOMO–LUMO energy levels and band gap, have been studied and discussed. In order to check the solid state properties, AIE studies were performed for some molecules. Attempts were also made to study and support the opto-electrochemical properties by theoretical DFT and TDDFT calculations. This tuneable molecular structure may be exploited for specific applications requiring D–A interactions and their resulting opto-electronic properties.

Results and discussion

Synthesis and characterization

The synthesis of the target compounds **2–9** based on 2,9-dibromo-6-ethyl-6*H*-indolo[2,3-*b*]quinoxaline (**1**) is illustrated in Scheme 1. The parent compound **1** required for the present study was synthesized by condensing 5-bromo-1-ethylindoline-2,3-dione and 4-bromobenzene-1,2-diamine, and the product was verified by ^{1}H NMR, ^{13}C NMR and mass spectra. 5-Bromo-1-ethyl-indoline-2,3-dione was prepared by a reported method.[17] The molecule **1** was appropriately modulated to various diaryl-amine/heterocyclic amine derivatives **2–9** by Buchwald–Hartwig coupling amination reactions[16] in the presence of tris-(dibenzylideneacetone)dipalladium ($Pd_2(dba)_3$) (5 to 8 mol%) as the palladium catalyst, SPhos (2-dicyclohexylphoshpino-2′,6′-dimethylbiphenyl) as a co-ligand and sodium *t*-butoxide (*t*-BuONa) as a base. The reaction mixture was continuously stirred for 5 to 12 hours under nitrogen atmosphere at 110 °C.

The reaction mixture was then cooled to room temperature and extracted with chloroform. The solid thus obtained was then purified by column chromatography (eluent: *n*-hexane: chloroform). The compounds **2–9** were obtained in 40% to 73% yield as yellow-red solids that are soluble in common organic solvents, including dichloromethane, toluene, methanol, and cyclohexane. Further, it was observed that the yield of the reaction was significantly affected by the substituents attached to the diarylamine; the presence of electron-withdrawing $-NO_2$ and –N=N–Ph groups on the diarylamine resulted in better yields compared to the presence of electron-donating $-OCH_3$ groups. The identity and purity of all target compounds were confirmed by ^{1}H and ^{13}C NMR spectroscopy, MALDI-TOF mass spectrometry, FT-IR spectroscopy, and elemental analysis. The melting points of **1–9** were determined by the open capillary method. The detailed synthetic procedure and characterization data of compounds **1–9** are given in the Experimental section.

Photophysical properties

The nature of the solvents and molecular structures have great effects on absorption and fluorescence spectra. Consequently, herein, we studied the solvent-dependent absorption and emission properties of **1–9** by UV-visible and fluorescence spectroscopy using toluene, chloroform (CHL), dichloromethane (DCM), tetrahydrofuran (THF) and dimethyl sulfoxide (DMSO) as solvents with varying polarities. Absorption and emission spectra of **2–9** in toluene and DCM are shown in Fig. 2 and 3 (for the other spectra, see Fig. S1 and S3–S7, ESI†). The pertinent photophysical data are summarized in Tables 1 and 2.

Influence of molecular structure on the absorption spectra

The molecular structure of a chemical compound has a profound influence on its UV/vis absorption properties, with changes in the position, intensity, and shape of the absorption bands.[18] Consequently, to check the structure–property relationships, absorption spectra were recorded at a concentration of 1×10^{-5} mol L^{-1} in various solvents, as depicted above (Fig. 2 and Fig. S1 and S3–S7(a), ESI†). All synthesized compounds

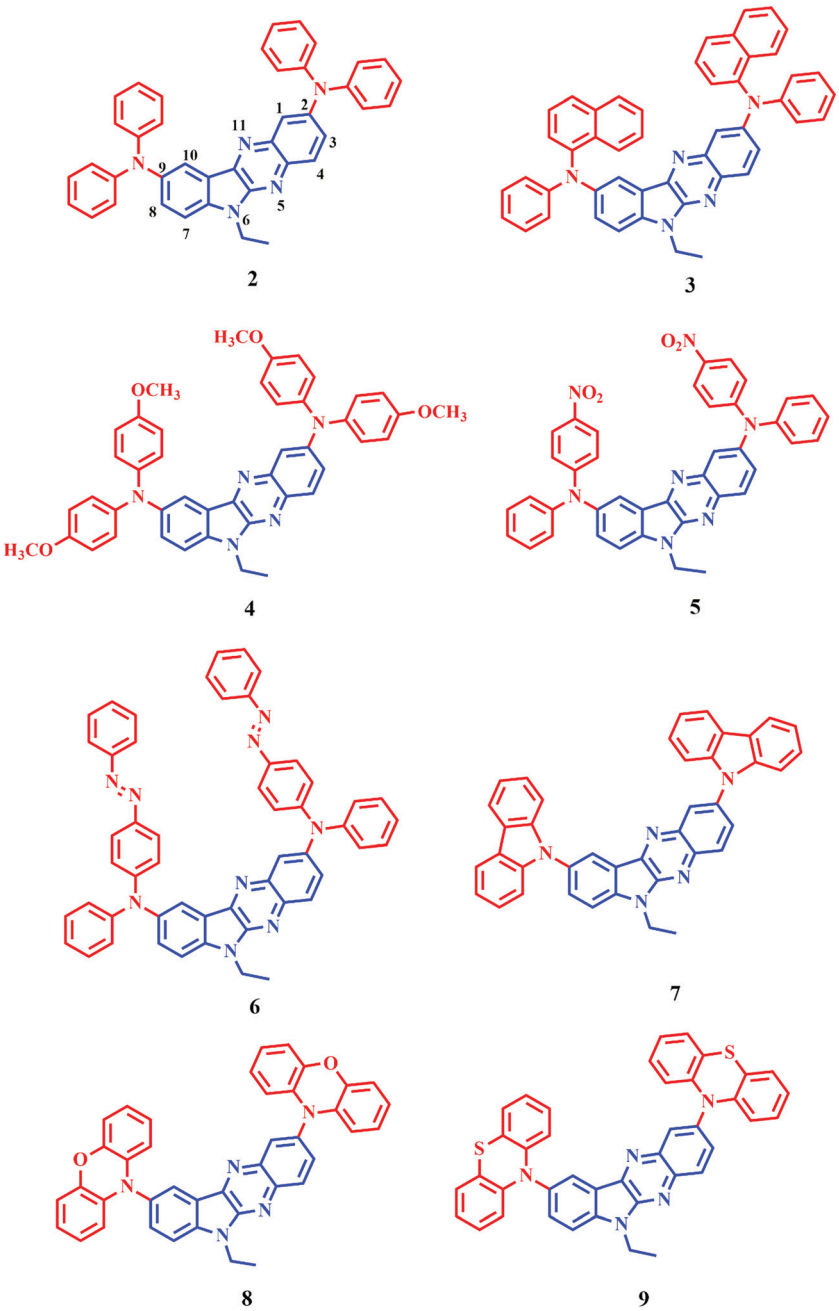

Fig. 1 Molecular structures of the indolo-quinoxaline amine derivatives.

show better absorbance and high molar absorptivity in all solvents (Table 1).

The multiple overlapping bands observed in the absorption spectra of **1** indicate the presence of non-conjugated chromophoric segments. The electronic spectra of **1** possess higher energy n–π* and π–π* (λ_{max} = 283 to 363 nm) transitions, which is a feature of vibrionic patterns; this originates from the entire indolo-quinoxaline unit and lower energy ICT (λ_{max} = 411 to 416 nm) transitions (Fig. S1(a), ESI†). The lower energy transition signifies inbuilt ICT character (exhibit D–A architecture) in **1**; this arises due to charge transfer between the electron-donating indole and the electron-accepting quinoxaline unit.

The charge transfer probability and donor ability of the indolo-quinoxaline segment in the D–A framework can be enhanced by introducing various amine units at the 2nd and 9th positions of **1**. Accordingly, the ICT band is red shifted by 18 to 26 nm in **2** and **3** with concomitant enhancements in the intensity compared to **1** due to the auxochromic effect exerted by the diarylamine unit (Fig. 2). The presence of the electron donating methoxy (–OMe) group on the diarylamine segment in **4** further improved the donating capacity and showed a more significant bathochromic shift than **2**. However, the electron withdrawing nitro ($-NO_2$) group and phenyldiazene (–N=N–Ph) segment on the diarylamine unit in **5** and **6**, respectively, show strong π-accepting

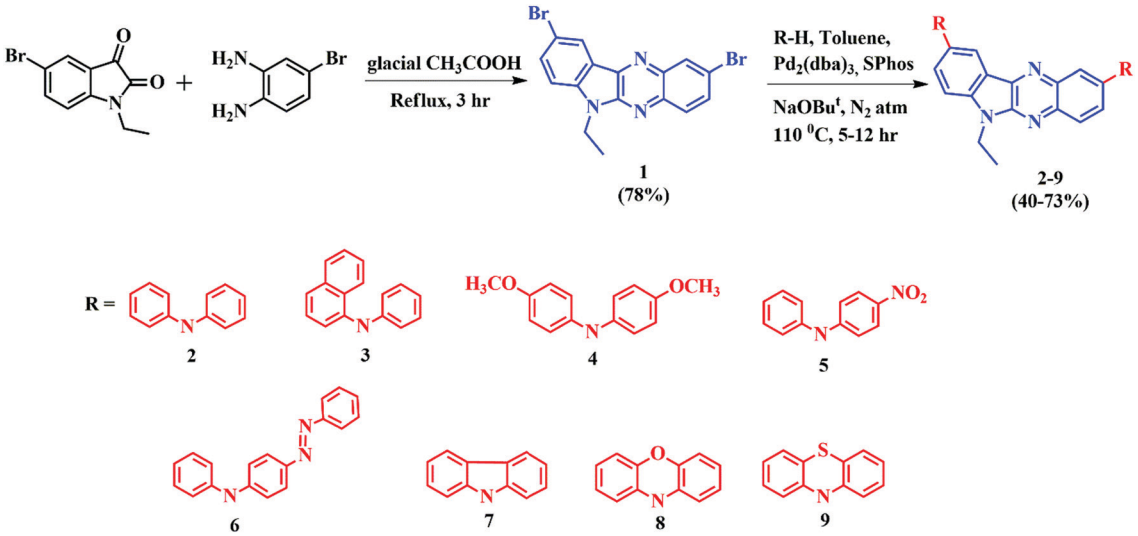

Scheme 1 Synthesis of indolo-quinoxaline amine derivatives **1–9**.

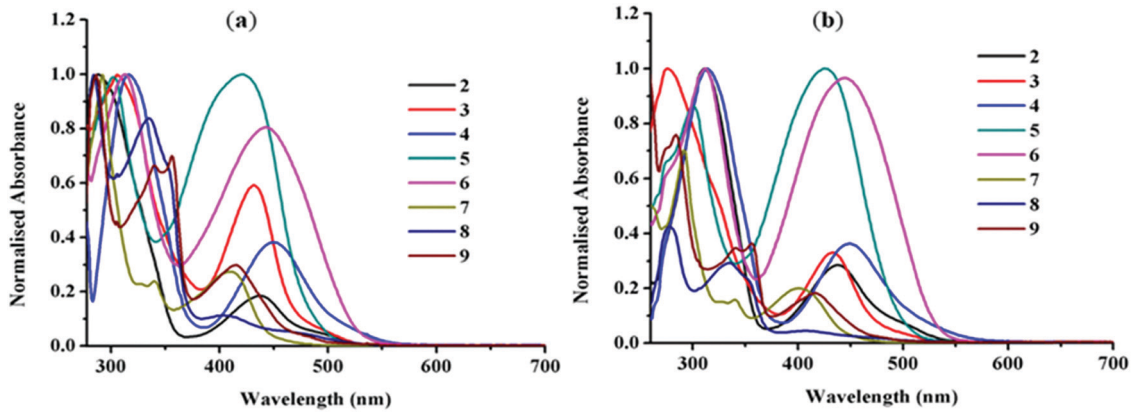

Fig. 2 UV-Vis absorption spectra of compounds **2–9** in toluene (a) and DCM (b).

nature and may enable charge transfer contributions from the amine to the nitro/phenyldiazene segment, which leads to intense charge-transfer bands (Fig. 2 and Fig. S3–S7(a), ESI†). In addition to its strong π-accepting nature, the negative inductive (−I) effect possessed by the $-NO_2$ substituent in **5** decreases the electron density at the tertiary nitrogen atom of the amine by withdrawing

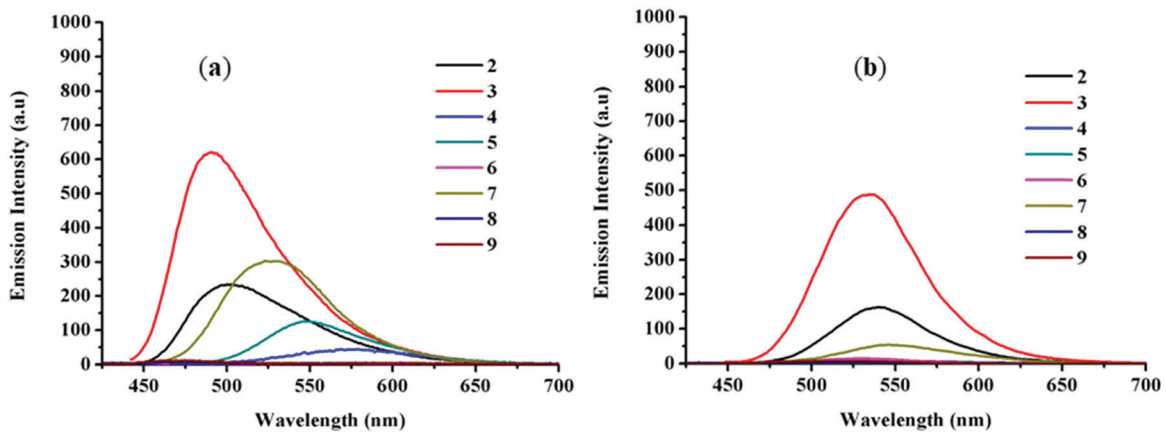

Fig. 3 Emission spectra of **2–9** in toluene (a) and DCM (b) (for other solvents, see Fig. S3–S7(b), ESI†).

Table 1 Absorption data of **1–9**

	λ_{abs}[ab], nm (log ε_{max} M^{-1} cm^{-1})					
Dye	Toluene	DCM	CHL	THF	DMSO	Solid film
1	284 (5.03) 344 (5.36) 361 (5.27) 412 (6.03)	286 (5.00) 344 (5.39) 361 (5.25) 414 (6.03)	286 (5.01) 345 (5.39) 361 (5.27) 411 (6.05)	283 (4.77) 346 (5.39) 360 (5.24) 416 (6.04)	286 (4.97) 346 (5.41) 363 (5.25) 416 (6.02)	292 373 441
2	289 (4.99) 437 (5.72)	311 (5.20) 438 (5.75)	312 (5.11) 442 (5.65)	300 (4.97) 434 (5.59)	299 (5.14) 438 (5.75)	329 449
3	306 (5.29) 432 (5.52)	276 (5.12) 433 (5.60)	310 (5.10) 438 (5.32)	306 (5.09) 429 (5.33)	306 (5.26) 433 (5.52)	315 442
4	316 (4.09) 450 (5.51)	314 (4.96) 449 (5.41)	311 (5.19) 454 (5.65)	279 (4.73) 445 (5.58)	318 (5.04) 447 (5.46)	331 462
5	302 (5.39) 422 (5.39)	300 (5.42) 425 (5.35)	301 (5.12) 428 (4.99)	276 (4.67) 417 (5.05)	295 (5.34) 423 (5.33)	304 447
6	313 (5.33) 443 (5.42)	312 (5.30) 444 (5.32)	306 (5.13) 447 (5.23)	306 (4.96) 439 (5.44)	309 (5.24) 445 (5.37)	323 460
7	292 (5.19) 340 (5.81) 410 (5.75)	292 (5.06) 340 (5.70) 402 (5.60)	292 (5.00) 340 (5.13) 407 (5.54)	290 (4.89) 339 (5.64) 400 (5.54)	292 (5.34) 339 (6.06) 401 (5.98)	298 415
8	284 (5.05) 335 (5.12) 404 (5.99)	278 (4.99) 334 (5.70) 407 (5.60)	276 (4.66) 335 (5.31) 403 (6.12)	276 (4.86) 332 (5.34) 404 (6.14)	281 (5.09) 336 (5.14) 411 (5.98)	281 341 404
9	286 (5.21) 340 (5.39) 356 (5.37) 416 (5.73)	284 (5.08) 341 (5.42) 356 (5.40) 416 (5.70)	283 (5.19) 340 (5.18) 356 (5.62) 417 (5.93)	276 (4.71) 339 (5.54) 354 (5.34) 413 (5.86)	286 (5.08) 342 (5.42) 358 (5.46) 417 (5.68)	288 360 423

[a] Recorded in 10^{-5} M solution. [b] ε is the extinction coefficient (L mol^{-1} cm^{-1}) (in parentheses).

Table 2 Emission data, optical band gaps, Stokes shifts and quantum yields of **1–9**

	λ_{emi}[ab], nm, (E_g^{opt}, eV)					λ_{emi}, nm	Stokes shift[c], cm^{-1}, (ϕ_F (%))
Compd	Toluene	DCM	CHL	THF	DMSO	Solid film	Toluene
1	—	—	—	—	—	490	—
2	500 (2.63)	540 (2.49)	541 (2.56)	517 (2.57)	550 (2.44)	578	2883 (9.25)
3	491 (2.69)	536 (2.57)	537 (2.61)	507 (2.64)	544 (2.54)	573	2781 (12.96)
4	579 (2.42)	—	—	—	—	—	4951 (11.13)
5	548 (2.68)	—	—	510 (2.64)	—	566	5448 (1.85)
6	—	—	—	—	—	—	—
7	523 (2.64)	549 (2.59)	546 (2.63)	543 (3.00)	550 (2.70)	540	5269 (11.12)
8	—	—	—	—	—	592	—
9	—	—	—	—	—	600	—

[a] Recorded in 10^{-5} M solution. [b] Optical band gap (in parentheses) estimated using emission and excitation spectra $\left(E_g^{opt} = \frac{1240.8}{\lambda_{optedge}}\right)$ eV. [c] Quantum yield (in parentheses) with reference to quinine sulphate (ϕ = 0.54 in 0.1 M H_2SO_4).

the electron from the amine. As a result, the HOMO–LUMO energy band gap in **5** increased more than that of **2**, as evaluated by the electrochemical (Table 3) and theoretical data (Table 4); this leads to the blue-shifted ICT transition in **5**. The rigid structures of the cyclic amines in **7–9** have pronounced steric effects which decrease the donating strength of the amine on the indolo-quinoxaline core segment and show blue shifts in the ICT band compared to the other derivatives **2–6** bearing diarylamine moieties. The C–N linking behaviour of the *N*-phenyl carbazole in **7** affords weaker electron donating capacity to the conjugated backbone and endows the molecule with a more twisted conformation, with a ~34 nm blue shifted ICT band compared to **2**.[19] The extra oxygen in **8** and sulphur heteroatom in **9** from the phenoxazine and phenothiazine units, respectively, illustrate much stronger electron-donating ability than the *N*-phenyl carbazole unit in **7**. Consequently, stronger and broader ICT bands are expected in these molecules than in **7**;[6b,7d] this was validated by the absorption spectra of **2–9** in various solvents (Fig. 2 and Fig. S3–S7(a), ESI†), where the ICT band

Table 3 Electrochemical and thermal data of **1–9**

Compd	$E_{oxi}^{peak\,a}$	$E_{red}^{peak\,b}$	HOMO[c]	LUMO[d]	$E_g^{EC\,e}$	T_m[f] (°C)	T_d[g] (°C)
1	1.23, 1.89	−0.98, −1.44	−5.66	−3.56	2.1	205	255 (275)
2	0.95, 1.29, 1.51, 1.77	−0.91, −1.51	−5.42	−3.64	1.78	196	295 (382)
3	0.99, 1.33, 1.52, 1.71	−0.93, −1.59	−5.41	−3.64	1.77	189	173 (370)
4	0.77, 1.04, 1.28, 1.55	−0.87, −1.56	−5.18	−3.62	1.56	210	310 (420)
5	1.22, 1.57, 1.85	−0.86, −1.17, −1.51	−5.65	−3.71	1.94	203	245 (365)
6	1.05, 1.33, 1.55, 1.80	−0.84, −1.31, −1.52	−5.41	−3.69	1.72	214	230 (360)
7	1.43, 1.55, 1.76	−0.93, −1.45	−5.85	−3.64	2.21	198	250 (410)
8	0.97, 1.24, 1.56, 1.75	−0.87, −1.55	−5.38	−3.66	1.72	184	350 (450)
9	0.94, 1.28, 1.62, 1.83	−0.89, −1.45	−5.35	−3.68	1.67	192	215 (270)

[a] E_{oxi}^{peak} oxidation peak potential (V). [b] E_{red}^{peak} reduction peak potential (V). [c] HOMO energy level calculated from $E_{HOMO} = -[E_{oxi}^{peak} - E_{redox}\,(Fc/Fc^{+}) + 5.1]$ eV. [d] LUMO energy level calculated from $E_{LUMO} = -[E_{red}^{peak} - E_{redox}\,(Fc/Fc^{+}) + 5.1]$ eV. [e] E_g^{EC} calculated from $E_g^{EC} = [HOMO - LUMO]$ eV. [f] Melting point determined by open capillary method. [g] Decomposition temperatures at 5% and 10% (in parentheses); weight losses derived by TGA.

Table 4 Computed electron affinities, ionization potentials, wavelengths, oscillator strengths, main vertical electronic transitions, orbital energies and dipole moments (μ_g) of **1–9**

Compd	E_a (eV)	I_p (eV)	λ_{max} (nm)	F	Assignments	E_{HOMO} (eV)	E_{LUMO} (eV)	E_g (eV)	μ_g
1	1.22	7.49	426.52	0.0418	HOMO → LUMO (69.90%)	−6.15	−2.63	3.51	4.81
			349.83	0.0029	HOMO–4 → LUMO (70.13%)				
2	0.96	5.98	544.63	0.0396	HOMO → LUMO (70.22%)	−4.99	−2.18	2.18	1.66
			359.65	0.0310	HOMO−2 → LUMO (70.18%)				
					HOMO → LUMO+1 (70.18%)				
3	0.91	5.95	530.70	0.0295	HOMO → LUMO (70.18%)	−4.99	−2.09	2.89	0.86
			407.07	0.0828	HOMO−1 → LUMO+2 (21.07%)				
					HOMO → LUMO+2 (66.20%)				
4	0.83	5.59	593.81	0.0255	HOMO → LUMO (70.32%)	−4.64	−2.02	2.62	2.38
			374.55	0.1148	HOMO−2 → LUMO (50.22%)				
					HOMO → LUMO+1 (46.92%)				
5	1.73	6.66	505.48	0.1225	HOMO → LUMO (57.50%)	−5.72	−2.76	2.95	13.28
6	1.55	6.02	543.01	0.1186	HOMO → LUMO (58.11%)	−5.17	−2.42	2.74	4.11
7	1.28	6.49	490.61	0.0460	HOMO → LUMO (70.14%)	−5.52	−2.55	2.96	4.22
			397.90	0.0003	HOMO−3 → LUMO (70.33%)				
8	1.38	5.96	644.06	0.0062	HOMO → LUMO (70.41%)	−4.95	−2.67	2.28	5.52
			407.87	0.4540	HOMO−2 → LUMO (69.68%)				
9	1.37	6.27	544.70	0.0005	HOMO → LUMO (70.27%)	−5.28	−2.64	2.63	4.02
			411.04	0.0437	HOMO−2 → LUMO (69.82%)				

extended to longer wavelengths in **8** and **9**, as expected. The extended ICT band suggests that the HOMO/LUMO spatial distributions have a higher extent of separation of the electron donor (phenoxazine/phenothiazine) from the electron acceptor group in these compounds; this was demonstrated by the HOMO and LUMO orbital diagrams (Fig. S48, ESI†) obtained computationally, as explained in the Theoretical section. Further, the larger charge separation also revealed that the poor electronic interaction between the donor and acceptor moieties due to its twisted conformation and that the lone pair of electrons on the nitrogen did not effectively overlap with the acceptor moiety, which results in broader and stronger ICT bands, as shown in **8** and **9**.[13b,20] However, phenothiazine has stronger donor ability than phenoxazine, which leads to the broader ICT peak in **9** than in **8** (Fig. 2).

Thus, the absorption properties of a particular dye largely depend on the type of substituents and the resulting electronic communication between the donor and acceptor. Therefore, these properties can be enhanced by modulating the electron donating strength of the peripheral amine on the indolo-quinoxaline segment. The order of increasing electron donating strength of the peripheral amine on the indolo-quinoxaline segment is based on the magnitude of the bathochromic shift that occurs in the ICT transition. However, absorption property was found to be ineffective on increasing the solvent polarity.

Impacts of donor groups and solvents on the emission spectra

The extent of the solvatofluorochromic effect in polar molecules is based on the change in the dipole moment of the molecule in the first excited state and ground state during excitation. The electron transition from S_0 to S_1 by excitation of the molecule decreases their energy gap because of the solvation. This decrease in the energy gap depends on the dipole moments of S_0 and S_1 as well as the solvent polarity. Meanwhile, it is generally known that the dipole moment of S_1 is larger than that of S_0, which directly results in an increase in the Stokes shift from non-polar solvent to polar solvent due to decreased self-reabsorption. In the case of D–A molecules, in addition to locally excited (LE) emission, ICT emission is observed. In these cases, the polar solvent is more likely to solvate the excited state of the ICT, which further decreases the energy gap by stabilizing the enhanced dipole moment of the excited state and results in red-shifted emission.[18,21] The larger

the dipole moment change, the greater the red shift of the emission/solvatofluorochromic effect. This red shift in emission with increasing solvent polarity by stabilization of the excited state is known as positive solvatochromism, where fluorescence bands are more greatly influenced by changes in solvent polarity than the corresponding absorption bands.[18] Thus, negligible effects on the ICT transition of **2–9** were found with increasing solvent polarity, which suggests that the ground-state electronic structures are independent of changes in the solvent polarity but depend on the relative strength of the substituted donor moiety (Fig. 2 and Fig. S3–S7(a), ESI†). Meanwhile, eminent solvatochromism was observed in the emission spectra from nonpolar to polar solvent (Fig. 3 and Fig. S3–S7(b), S9, ESI†).

The origin of emission in **2–9** is efficient energy migration from the excited state of the peripheral amine segment to the indolo-quinoxaline reservoir. Compounds **2–9** emit at 491 to 579 nm in toluene (polarity index (PI) = 2.4, dipole moment (μ) = 0.31), whereas in polar aprotic solvents such as DCM (PI = 3.1, μ = 1.14) and chloroform (PI = 4.1, μ = 1.15) positive solvatochromism was witnessed by red shifts of 30 to 45 nm and 33 to 46 nm, respectively (Table 2, and Fig. S3–S6(b), S9(a–d), ESI†). However, negative solvatochromism was witnessed in **2–9**, with blue shifted emission in THF (PI = 4.0, μ = 1.75) solvent compared to in chloroform; this may arise because the ground state is more polar than the excited state. In negative solvatochromism, stabilization of the ground state molecule is greater than that of the excited state due to the solvation of polar solvents or H-bonding interactions between the solute and solvent molecules; this increases the energy gap between the excited and ground states, resulting in a blue shift.[18]

In the case of highly polar solvents such as DMSO (PI = 7.2, μ = 4.1) (Fig. S7(b) and S9(e), ESI†), molecules **2–9** experience nonradiative relaxations due to the formation of excimers, which causes more quenching of the emission than in nonpolar solvent. In addition to the nonradiative relaxation, the excited state of a luminophore may be quenched by several physical processes, such as photo-induced electron transfer (PET), resonance energy transfer to a quencher, dipole–dipole interactions, and complex formation.[2a]

In addition to the change in dipole moment, the electron donating and accepting ability of a dye to or from surrounding solvent molecules in its ground and excited states further establish its solvatochromic effects.[7d,18,22] This dependency of emission behaviour on the surrounding medium was witnessed in the cases of **2–9** due to the presence of different amines as donor segments on the indolo-quinoxaline core unit. As a consequence, molecule **2** bearing diphenylamine as a donor group emits green colour at 500 nm in toluene, whereas molecule **3** emits at 491 nm due to the presence of the bulky naphthyl ring, which increases π–π steric hindrance within the molecule. The polar nature and strong electron donating ability of the $-OCH_3$ group in **4** increases the electron density on the tertiary nitrogen atom of the diarylamine, which leads to restricted rotation of the phenyl groups in polar solvent. Thus, compound **4** emits only in toluene at 579 nm, with a distinct bathochromic shift compared to the other derivatives (Fig. 3), and shows quenching phenomena in polar solvents such as DCM, CHL, THF and DMSO due to polar-polar interactions.[23] The stronger ICT effects possessed by **5** and **6** decrease the bandgap between the ground and Franck–Condon excited states, with a more red-shifted emission band than **2**, and assist non-radiative decay, resulting in decreased/quenched fluorescence. Dye **7** shows a greater red shift in its emission than **2** due to its mirror symmetry of absorption and emission spectra due to loss of vibrational excitation energy during the excitation/emission cycle, as suggested in the Franck–Condon principle and Kasha's rule for organic dye molecules.[24] In the cases of **8** and **9**, the number of π electrons in the middle rings involving O/S and N is eight; therefore, the electron delocalization of the heteroatoms is inefficient, and the two benzo-fused rings of phenoxazine and phenothiazine may retain their individual aromaticity.[7d] This ineffective electron delocalization of the heteroatoms due to the aromaticity of **8** and **9** may accomplish quenching behaviour in all solvents. Moreover, formation of collision complexes or exciplexes in **8** and **9** by the photo-induced electron transfer process in the D–A model from the strong electron donating phenoxazine and phenothiazine units to the indolo-quinoxaline moiety may also result in quenching.[7d,25]

The Stokes shifts in **2–9** were found to be 2781 to 6755 cm^{-1} and to increase with increasing polarity of the solvent (Table 2 and Tables S2–S9, ESI†), which confirms that there is no reabsorption of the emitted photons. The larger Stokes shifts in **2–9** suggest that the origin of the emission is mainly based on strong intramolecular charge transfer between the donor and acceptor units. The optical band gaps of **2–9** calculated by the intersections of the emission and excitation spectra are in the range of 2.42 to 3.00 eV (Table 2). The quantum yields of **2–9** were calculated using quinine sulphate (ϕ = 0.54 in 0.1 M H_2SO_4) as a reference. The observed low quantum yields for **2–9** even in toluene suggest a prominent nonradiative deactivation pathway for the excited state (Table 2 and Tables S2–S9, ESI†).

Absorption and emission behaviour of 2–9 in neat solid films

For practical application of a D–A molecule, it should be emissive in the solid/aggregate state. Thus, to check the optical properties of **2–9** in the aggregate state, UV/vis. absorption and fluorescence studies of their neat solid films were performed. The slightly higher and broader absorption maxima (Fig. S8(a), ESI†) in **2–9** than in the solution state (Fig. 2, and Fig. S3–S7(a), ESI†) with bathochromic shifts of the ICT band suggest that intermolecular aggregation occurred in the neat solid films. Similarly, the solid film emission maxima (540 to 600 nm) in **2–9** (Fig. 4 and Table 2) were found to be more red-shifted than in the solution state (Fig. 3, Fig. S3–S7(b), ESI† and Table 2), which is a primary indication of the formation of aggregates. Here, almost all the compounds showed more or less intense emissions in the neat solid films except **4** and **6**. In the cases of **4** and **6**, the solid state emission was quenched due to enhancement of the intermolecular D–A interface by fast interchain electron transfer from the donor to acceptor subunits *via* close spatial contact.[26]

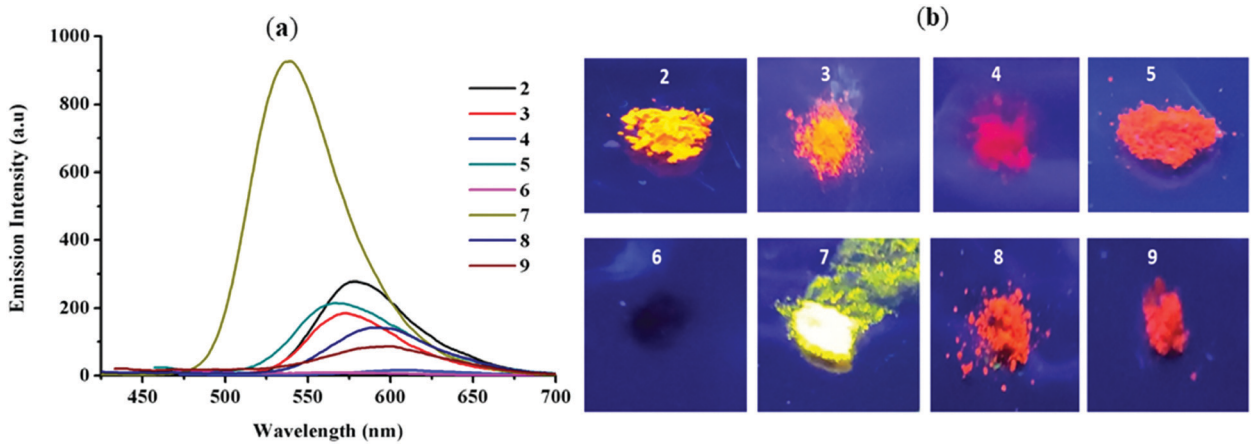

Fig. 4 Emission spectra of **2–9** in neat solid films (a), images of solid powders (b) of **2–9** under a UV lamp (365 nm).

The optimized geometries obtained by computational studies of **2** and **7** (Fig. 9) suggest that both molecules have a 'pyramid mimicked' configuration.[27] However, the major structural difference between them is based on the difference in their rotational freedoms in organic solvent, which mainly affects the ICT band. The rotational freedom of the diarylamine in **2** is higher than that of the rigid carbazole unit in **7**, which in turn effectively decreases the rotation. In this case, co-facial alignment of the molecules is prevented by rotation of all phenyl rings to some degree between each other and hinders excimer formation, which leads to solid state emission by aggregate formation. Henceforth, the mimicked configuration can effectively prevent π–π interactions in the solid state and limit aggregation quenching in **2** and **7**.[27] However, molecule **7** was found to be more highly emissive in the solid state than **2** due to its twisted conformation and increase in intermolecular interactions.[27,28] However, dyes **8** and **9** were found to be non-emissive in the solution state but emissive in the solid state due to the adoption of a non-planar spatial conformation at their optimized lowest energy states; this prohibits close packing and π–π interactions in the solid state, resulting in fluorescence emission.[29] The non-planar spatial conformations exhibited by phenoxazine and phenothiazine-based dyes **8** and **9** were confirmed by their optimized ground state molecular structures (Fig. S43, ESI†).

Usually, aggregation caused by strong intermolecular π–π interactions between neighbouring groups and the formation of less emissive excimer species with non-radiative relaxation processes in the solid phase debases or decreases their emission efficiency more efficiently than in the solution state.[30] However, various molecules possess anomalous behaviour with intense solid state emissions during their solid state application in optoelectronic devices. This phenomenon is termed AIE and is caused by aggregate formation. AIE-active molecules are recognised as AIEgens and show different behaviour than ACQ molecules.

Consequently, it is assumed that the solid state emissions in the D–A pairs of luminogens **2**, **3**, **5**, **7**, **8** and **9** may exhibit AIE properties. Thus, to evaluate and understand whether this abnormal behaviour of the molecules is caused by aggregation, we studied the AIE characteristics of these molecules, as depicted in the following section.

AIE and size-dependent emissions in the nanoparticles

The AIE activities of the dyes were investigated by the formation of nanoaggregates/nanoparticles using a precipitation method without using surfactant.[31] All molecules under study are highly soluble in THF but insoluble in water, which suggests that solvent mixtures of these molecules with high water contents must contain aggregated particles. Using this concept, solutions of THF with increasing water percentages were prepared without altering the final concentration, *i.e.* 10 μM, to access the formation of nanoparticles using UV/vis and emission spectra.

The immiscibility the of dye molecules at high water fractions (f_w) in the THF/water mixture creates a hydrophobic environment, which results in the formation of aggregates. However, homogeneous mixtures with no precipitate of aggregates in the solution imply that the aggregates are nanoscale and can hence be called nanoparticles[11] (Fig. 5(c)). Further, the UV-Visible spectra (Fig. 5(a) and Fig. S10, ESI†) of the dyes in THF/water mixtures with high water fractions (f_w) showed increases in the absorption intensity with extended wavelength or level-off tail characteristics due to the presence of "Mie-scattering," which signifies that the nanoparticle formation is due to their hydrophobic nature[32] (*i.e.* poor solubility of dye molecules in water). The dynamic light scattering (DLS) data of all dye molecules under study (Fig. S12, ESI†) confirmed the presence of nanoparticles in homogeneous suspensions of the THF–H_2O mixture. Homogeneity in the homogeneous suspensions of the THF–H_2O mixtures was confirmed by the low polydispersity indices (PDI) obtained by DLS data.

The presence of strong intramolecular forces between the donor and acceptor moieties of **2**, **3**, **5** and **7** leads to emission in pure THF solution. However, dyes **8** and **9** were non-emissive in pure THF/any solvent; this may be due to aromaticity or the photo-induced electron transfer process, as explained in the above section. Later, gradual increment of the percent of water

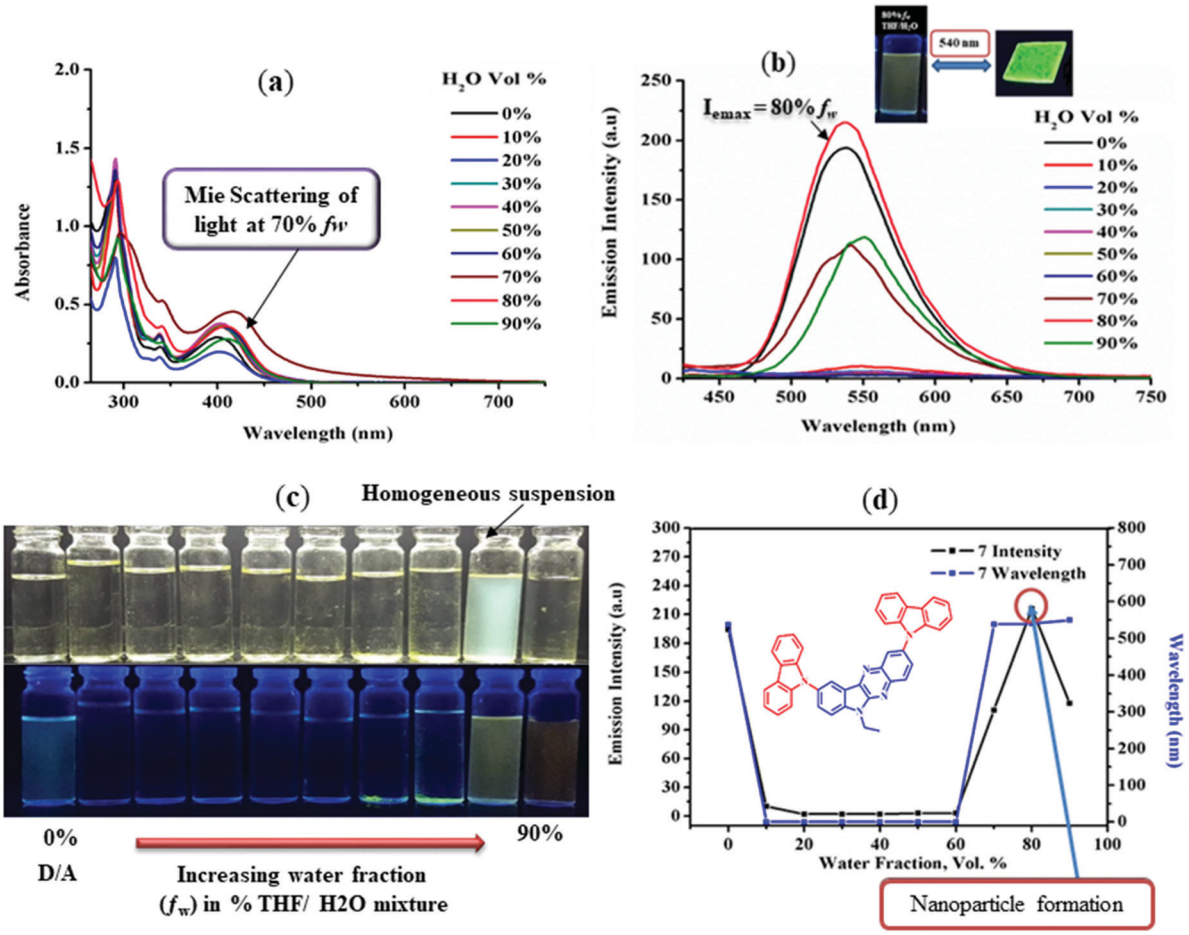

Fig. 5 Absorption (a) and emission (b) spectra of **7** in THF–H_2O mixtures (10 μM) with different water fractions (f_w) excited at 400 nm; (c) emission images of **7** showing AIE effects in THF–H_2O mixtures (10 μM) with different % water fractions (f_w). (d) Plots of wavelength and emission intensity *versus* % of water fraction of **7** in THF/water mixtures.

in the THF solution up to an 80% water fraction (f_w) decreased the emission intensity in **2** and **3** (Fig. S11(a) and (b), ESI†). Further addition of water (90% f_w) enhanced the emission intensity slightly, implying the formation of nanoparticles due to the hydrophobic environment. The formation of nanoparticles at high water content (90% f_w) restricts intramolecular rotational (RIR) and vibrational motions and blocks the non-radiative decay pathway of the excited state or the formation of less emissive excimer species; this allows the molecules to exhibit fluorescence efficiently.[33] Conversely, in the case of **5** (diarylamine linked with $-NO_2$ chromophore at the para position), enhancement of the emission intensity was found at 70% f_w, and it continued to increase up to 90% with a bathochromic shift compared to pure THF solution; this is attributed to different conformations, random packing modes and morphological changes in the aggregated state.[34] Hence, due to the increases in emission intensity at high water content, molecules **2**, **3** and **5** are AIE-active fluorophores which overcome the ACQ problem. However, the extent of AIE activity in **2**, **3** and **5** was found to be weak; thus, they can be called weakly AIE-active molecules. Further, the formation of nanoparticles in homogeneous suspensions of 90% f_w THF–H_2O mixtures were confirmed by DLS data, with hydrodynamic average sizes of 81 nm in **2**, 144 nm in **3** and 91 nm in **5**.

In the case of **7**, the emission in THF solution was turned off in the water fraction range from 10% to 60% (Fig. 5(b)–(d)) due to its twisted conformation. The emission turned on when the water fraction reached 70% due to the formation of nanoparticles and continued to increase up to 80% f_w (I_{max}) in THF solution due to the RIR effect (Fig. 5(b)–(d)). The hydrodynamic average size of the nanoparticles formed at 70% f_w was 414 nm and that at 80% f_w was 115 nm as obtained by DLS (Fig. 6(b) and Fig. S12(d) and (e), ESI†). After 80% f_w in the mixture, a slight drop of the emission intensity (Fig. 5(b)) was observed due to the formation of less emissive nanoparticles[34] with an average size of 254 nm (Fig. S12(f), ESI†). The variation in hydrodynamic size with percentage of f_w was due to the different conformation packing of the aggregated state formed in the THF–H_2O mixture. Thus, molecule **7** showed nanoparticle size-dependent emission behaviour. Further, the size and morphology of the observed nanoparticles in the case of **7** were examined using field emission gun scanning electron microscopy (FEG-SEM). The nanoparticles obtained at 80% f_w of the THF–H_2O mixture were circular, with a mean diameter about 28 to 140 nm in scale (Fig. 6(a)).

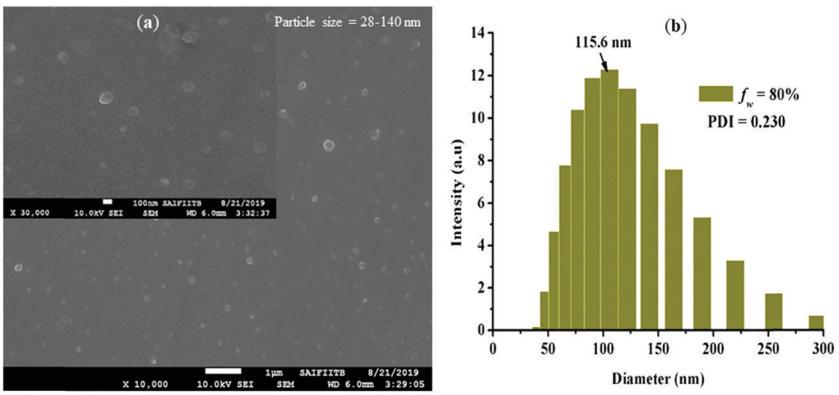

Fig. 6 FEG-SEM image of the nanoparticles (a) and DLS plot (b) of **7** obtained from an 80% f_w THF–H_2O homogeneous suspension.

Compared to the other derivatives, molecule 7 has robust AIE activity due to the conformationally restricted rotation of carbazole compared to the diarylamine segment; it exhibits astonishingly higher solid-state emission than solution state emission due to the formation of nanoparticles. Strikingly, the emission wavelength of 7 from the 80% f_w THF–H_2O mixture (540 nm) precisely matches the solid film emission maximum, *i.e.* 540 nm (Table 2 and Fig. 5(b)). This observed feature establishes the formation of nanoparticles and diminishes the solvatochromic effect at high water percentage in the THF–H_2O mixture.[35]

Although molecule **9** shows solid state emission, it was found to be AIE inactive. The reason for the AIE inactivity in this molecule may be the covalent locking conformation of the phenyl rings by a sulphur bridge.[23] Increase in the water fraction leads to formation of precipitation which is non-emissive in UV light (365 nm). The precipitation could even be seen by the naked eye, probably due to the limited solubility of the molecule in water.[21] A similar trend was observed in the case of **8**, which was found to be an AIE-inactive dye. However, the precipitated particles formed by increasing the water fraction to 80% were found to have diameters of 284 nm in **8** and 133 nm in **9** as obtained by DLS data (Fig. S12(g) and (h), ESI†).

Therefore, different donor-substituted molecules show different types of AIE or ACQ activity with varying size of the nanoparticles depending upon their morphology and the fraction of water. This sensitive method of formation of organic nanoparticles with on/off switching of light emission suggests possible solid state application of these molecules in opto-electronic devices.

Electrochemical properties

Materials with D–A architectures have a propensity to stabilize both cations and anions due to their charge-transport capability and feasibility of electron injection and transport; this can be estimated by electrochemical/cyclic voltammetry measurements. Accordingly, cyclic voltammetry (CV) measurements of **2–9** were performed in dichloromethane with 0.1 M tetrabutylammonium hexafluorophosphate as the supporting electrolyte in a conventional three-electrode assembly using Ag/AgCl as a reference electrode and ferrocene as an internal standard to calibrate the redox potentials. The analogous redox potentials of **1–9** are listed in Table 3, and cyclic voltammograms of **2** and **7** are shown in Fig. 7. The repeated scan of the CV wave did not undergo substantial modification, revealing that all dyes were electrochemically stable under oxidative and reductive conditions.

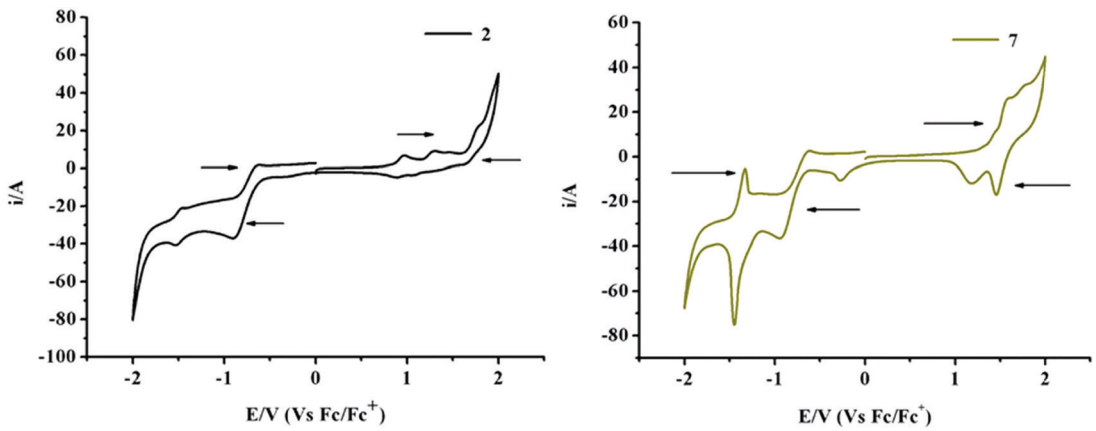

Fig. 7 Cyclic voltammograms (full scan) of **2** and **7** (for the other compounds, see Fig. S12, ESI†).

The anodic sweep cyclic voltammogram of compound **1** shows an irreversible first oxidation wave at 1.23 V, probably originating from the indole subunit. A second oxidation wave at a higher oxidation potential was seen at 1.89 V; this may be due to oxidation of the indolo-quinoxaline core moiety. Meanwhile, substitution of different amine (chromophore) substituents as donors on 6*H*-indolo[2,3-*b*]quinoxaline extends the D–A interaction and improves the oxidation peaks of the indole segment towards the more positive side. Accordingly, derivatives **2–9** show oxidative potential of the indole segment in the range of 1.28 to 1.62 V and of the indolo-quinoxaline core unit at 1.55 to 1.85 V. In addition, the molecules bearing amine substituents except **5** and **7** have two additional quasi-reversible peaks in the range of 0.77 to 1.33 V, and one quasi-reversible wave was observed for **5** (1.22 V) and **7** (1.43 V).

This lower oxidation potentials displayed by **2–9** towards lesser positive potentials than **1** are attributable to the oxidation of the peripheral amines at the 2nd and 9th position of the 6*H*-indolo[2,3-*b*]quinoxaline core. Less oxidation potential was observed for **4** at 0.77 V than for other derivatives due to the strong electron-donating effect possessed by the $-OCH_3$ group present on the diarylamine segment. However, higher oxidation potential at 1.43 V was shown by **7** due to the rigid (cyclic) carbazole substituent on the indolo-quinoxaline core segment. Meanwhile, phenoxazine (in **8**) and phenothiazine (in **9**) amine substituents have a tendency to form stable radical cations and anions due to their larger charge separation from the indolo-quinoxaline core, which is explained by the PET phenomenon; they show strong donating effects with lower oxidation potentials than **7**, namely 0.97 V and 0.94 V, respectively. Thus, the above data reveal that the oxidation potential is extremely sensitive to the nature of the corresponding donor group; the oxidation potentials of **2–9** decrease with increasing donor strength (**4** > **9** > **2** > **8** > **3** > **6** > **5** > **7**).

Further, a negative scan of **1** at the cathode shows two quasi-reversible waves at −0.98 V and −1.44 V, which may correspond to the formation of mono and diradical anions of the quinoxaline unit.[36] Similarly, amine-substituted derivatives **2–9** also show two quasi-reversible waves, one at −0.84 V to −0.93 V and the second at −1.45 V to −1.59 V. One additional reduction potential was observed for **5** (−1.17 V) and **6** (−1.31 V), corresponding to the reduction of the $-NO_2$ and –N=N– segments, respectively, attached to the diarylamine unit. However, it is known that quinoxalines linked with electron-withdrawing groups display facile reversible reduction couples.[37]

On the other hand, indication of quasi-reversible reduction in **2–9** suggests the role of electron-donating indole and amine segments, which probably decrease the electron affinity of the quinoxaline unit. Consequently, the reduction potential shifts cathodically with increasing donor strength of the amine.

The interfacial charge transport kinetics of materials in opto-electronic devices can be monitored by the HOMO and LUMO energy levels of that material. The HOMO and LUMO energy levels of compounds **2–9** were calculated from the first oxidation and reduction potentials. The HOMO and LUMO energy levels of compound **1** were found to be −5.66 eV and −3.56 eV, respectively. It is clearly evident that the nature of the amine unit significantly alters the HOMO/LUMO energies in **2–9** (Table 3); they were found to be in the ranges of −5.18 to −5.85 eV and −3.62 to −3.71 eV, respectively. Thus, substitution of different donor amines at the 2nd and 9th positions of **1** controlled the oxidation potential, and **2–9** showed high HOMO energy levels compared to **1**, except **7**; meanwhile, the slightly changed LUMO values suggest the formation of strong D–A character. As a consequence, the energy band gaps were also found to be suppressed compared to **1** (except **7**) by substitution of different donor amines on the acceptor moiety (Table 3). The observed band gaps in **2–9** were in the range of 1.56 to 2.21 eV. An increase in the band gap was observed in compound **7** (2.21 eV), indicating weaker electron donating capacity of carbazole than the other diarylamine/heterocyclic amines due to its locking conformation. On the other hand, the strong electron donating abilities of electron-rich methoxy-substituted diphenylamine and phenothiazine are responsible for the small band gaps of 1.56 eV in **4** and 1.67 eV in **9**.[38] The lower band gap suggests the injection of both hole and electron transporting properties within a molecule.

A D–A assembly with low-lying LUMO and high-lying HOMO orbitals possesses highly hybridized frontier molecular orbitals and ambipolarity.[39] The efficiency and stability of small and polymeric n-type and ambipolar materials are based on the essentiality of the HOMO ($\geq$5.6 eV) and low-lying LUMO energy levels (LUMO values between −3.0 and −4.0 eV).[7d–f,13,40] Meanwhile, the HOMO and low-lying LUMO energy levels of **2–9** are comparable to those of commonly used/reported small ambipolar-type (electron and hole transporting) materials such as 6,13-bis(triisopropylsilylethynyl)-1,4,8,11-tetraazapentacene (TIPS-PEN derivative) (HOMO = −5.49 eV; LUMO = −3.68 eV),[41] 2,7-bis((trimethylsilyl)ethynyl)cyclopenta[*h*,*i*]aceanthrylene (HOMO = −5.32 eV; LUMO = −3.67 eV),[42] and 1,4-diketo-2,5-dihexyl-3,6-bis(4-ethylendioxythienyl)phenyl)pyrrolo[3,4-*c*]pyrrole (HOMO = −5.40 eV; LUMO = −3.68 eV),[43] and polymers such as poly[2-methoxy-5′3′7′dimethyloctyloxyl)-1,4-phenylenevinylene) (MDMO-PPV) (HOMO = −5.4 eV; LUMO = −3.2 eV),[44] poly[2,6-(4,4-bis-2-ethylhexyl)-4*H*-cyclopenta-[2,1-*b*-3,4-*b*]dithiophene-*alt*-4,7(2,1,3-benzothiadazole) (PCPDTBT) (HOMO = −5.3 eV; LUMO = −3.55 eV),[45] and 2,2′-bis{5-[2,5-(2-ethnylhexyl)-6-(5-cyano-thiophene-2-yl-pyrrolo[3,4-*c*]pyrrole-1,4-dione-3yl]thiophene} (DPP_2CN) (HOMO = −5.45 eV; LUMO = −3.74 eV).[46]

Hence, due to the close agreement of the energy levels of **2–9** with the values required for ambipolarity, they are promising candidates as an ambipolar materials for organic electronics. Therefore, electrochemical properties such as lower band gap and balanced dual charge transport properties are abundantly impacted by substitution of a strong donor (amine) on the acceptor unit in the D–A framework.

Thermal properties

The stability and lifetime of photo-electronic devices are greatly influenced by the thermal properties of dyes. Materials possessing good thermal stability and high decomposition temperatures are found to improve the device performance.

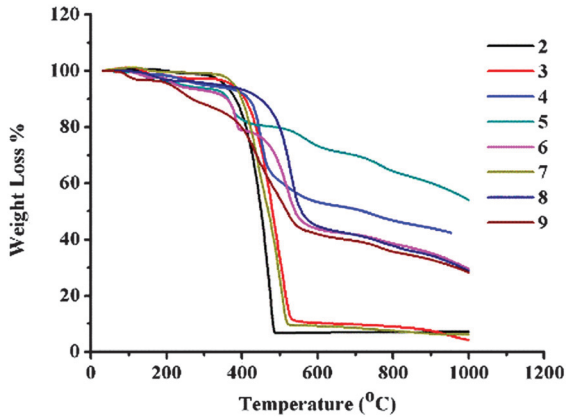

Fig. 8 Thermogravimetric plots of **2–9**.

The optoelectronic devices should withstand temperature increases as high as 80 °C.[47]

Subsequently, in order to study the thermal properties of molecules **2–9**, thermogravimetric analysis (TGA) was carried out. The observed thermal data of **2–9** are listed in Table 3, and the thermograms are displayed in Fig. 8. The thermogravimetric analysis revealed that compounds **2–9** are thermally stable materials with no weight loss at low temperature. The thermal decomposition temperatures of **2–9** corresponding to 5% and 10% weight loss are in the ranges of 173 °C to 350 °C and 270 °C to 450 °C, respectively (Table 3). The order of thermal stability of **2–9** is **8** > **4** > **2** > **7** > **5** > **6** > **9** > **3**. Thus, derivatives **2–9** have prospective usage in organic electronics due to their high thermal stabilities and decomposition temperatures.

Theoretical studies

To verify the molecular-level changes in the structure–property relationships with varying donor strength in **2–9**, detailed electronic studies were performed using density functional theory (DFT) and time-dependent density-functional (TDDFT) calculations. The molecular orbital levels and electrical properties of molecules **1–9** were calculated theoretically using the B3LYP/6-311G basis set as implemented in the Gaussian03 program.[48] The theoretically computed ground state frontier molecular orbitals and optimized structures of **2** and **7** are shown in Fig. 9 (for the other compounds, see Fig. S39–S48, ESI†). The Cartesian coordinates and Mulliken charges of **1–9** are given in Tables S10–S18 (ESI†). The main vertical electronic transition assignments for the most relevant singlet excited states, HOMO–LUMO orbital energies, energy gaps, vertical ionization potentials (IP), electron affinities (EA) and ground state dipole moments (μ_g) for all molecules are given in Table 4 (other assignments are shown in the ESI†).

In all of the molecules (Fig. S44–S48, ESI†), the HOMO energy levels were spread throughout the molecule except **8** and **9**, in which the HOMO orbitals are confined to the 2nd position of the heterocyclic amine moiety (Fig. S48, ESI†). Meanwhile, the LUMO is delocalized over the entire indoloquinoxaline segment in all dyes except for **5** and **6**. In the cases of **5** and **6**, the LUMO was extended from the indoloquinoxaline segment to the electron deficient –NO_2 (in **5**) and –N=N–Ph (in **6**)-substituted aryl ring of the amine segment attached to the 2nd position (Fig. S46 and S47, ESI†). The positions of the HOMO and LUMO orbitals in **2–9** clearly indicate the presence of D–A architectures, which is a feature of the ICT process.[49] Furthermore, the twisted conformation of **7** leads to less overlapping of the HOMO and LUMO orbitals than in **2** and confirms weak D–A interactions in **7**, as observed from the experimental absorption spectra (Fig. 2). Meanwhile, the HOMO/LUMO spatial distributions showed higher extents of charge separation for **8** and **9**, which disrupts the electronic communication between the donor and acceptor in the ground state and may lead to the PET process and suppression of the HOMO–LUMO energy gap.[50]

The HOMO and LUMO energy levels of **2–9** obtained by theoretical calculations are in the ranges of −4.64 to −5.72 eV and −2.02 to −2.76 eV, respectively, with energy band gaps from 2.18 to 2.96 eV (Table 4). The HOMO energies of **2–9** match well with the experimental values obtained by CV and predict facile hole injection from the anode (such as ITO) with a work function of ∼4.8 eV. However, the LUMO values and energy gaps are overestimated by about 1.0 eV. The overestimation may be due to ineffective interaction between the solvent and molecules. Additionally, the electronic properties obtained by theoretical calculations and experiments show similar impacts of the donor substituent on **1**. The energy band gaps obtained from the DFT calculations correlate with the optical band gaps and were found to decrease with increasing electron donating strength of the substituted diarylamines/heterocyclic amines in a similar fashion to the electrochemical data. Small band gaps were obtained computationally for dyes **4**, **8** and **9** due to the electron rich –OCH_3 group present on the diarylamine unit (in **4**) and due to the heterocyclic amines phenoxazine (in **8**) and phenothiazine (in **9**). However, molecule **7** with carbazole as a donor amine showed the highest theoretical and electrochemical band gaps among the derivatives. IP and EA were estimated by the differences in the total energies of the neutral and cationic/anionic species, respectively. Because electron-rich amines decreases the ionization energy, the lowest IP was observed for **4** with a –OCH_3 group on the diarylamine segment. The dipole moments of all the derivatives in the gaseous phase were found to be small except for **5** (13.28), whose dipole moment was large due to the presence of the polar –NO_2 group attached to diphenylamine. A small dipole moment of a dye implies that the dipole vectors cancel one another out due to their opposite directions.

It is well known that the HOMOs, LUMOs, and energy gaps of materials are directly related to their optical properties. Thus, in order to determine the precise optical properties of **2–9**, a TDDFT study was performed. Simulated electronic transition spectra of **1–9** obtained using the B3LYP/6-311G basis set are shown in Fig. 10. The transitions observed at high energies below 400 nm for all molecules correspond to n–π* and π–π* transitions involving the HOMO−1 and LUMO+1 orbitals (Table 4). Meanwhile, a transition above 400 nm

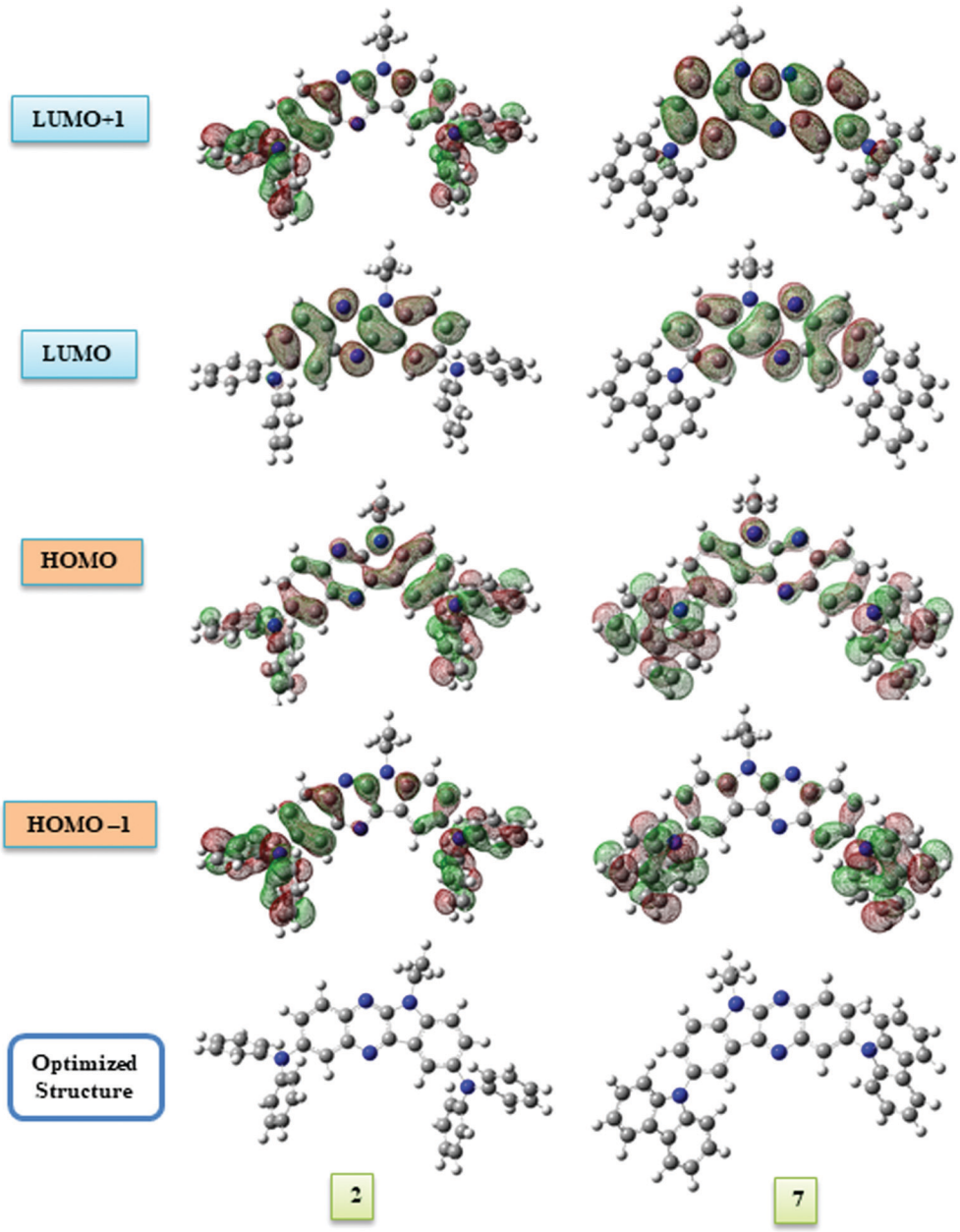

Fig. 9 Frontier molecular orbitals and optimized structures of **2** and **7**.

corresponds to ICT transitions with smaller oscillator strengths. The considerable red-shift for the theoretical vertical transitions is related to the self-interaction error in TDDFT arising from the electron transfer in the extended charge-transfer state.[51] Like the experimental data, bathochromic shifts in the ICT transitions were observed for compound **4**; this is attributed to the electron donating $-OCH_3$ group attached to the diphenylamine moiety. However, a low-intensity HOMO to LUMO transition was observed for **5** and **6**, which is in good agreement with the experimentally obtained parameters due to presence of electron withdrawing $-NO_2$ and –N=N–Ph groups on diphenylamine, respectively. Meanwhile, the heterocyclic amines in **7–9** show more blue-shifted ICT transitions than the other dyes, which implies weaker donor strength of the cyclic amines than the diarylamines.

Conclusion

indolo-quinoxaline-based D–A molecules **2–9** were synthesized and extensively studied to determine the effects of their substituted donor moieties on their photophysical, electrochemical and theoretical properties. The presence of ICT confirms the D–A assemblies in the dyes and was found to be considerably influenced by the donating nature of the substituted amines. Moreover, the emission maxima of the derivatives were also

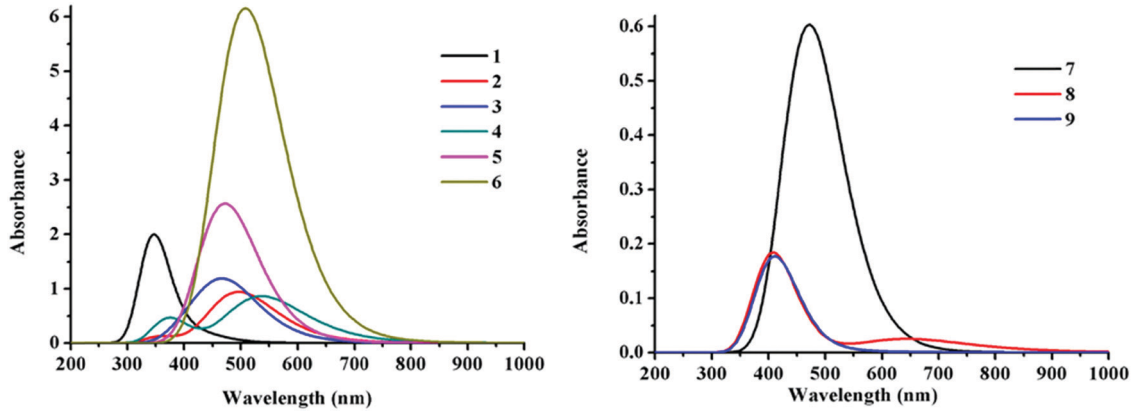

Fig. 10 Simulated electronic transition spectra of **1–6** (left) and **7–9** (right) obtained from the B3LYP/6-311G basis set.

altered by variation of the peripheral amines and solvents with different dipole moments, which led to positive/negative solvatochromism in the molecules. The dyes emit in the blue-orange region in solution and in neat solid films. Additionally, the solid state emission exhibits AIE properties in **2**, **3**, **5**, **7**, **8** and **9**, which reveals that AIE dominates the emission at higher water percentages due to the formation of nanoparticles, as confirmed by DLS. However, robust AIE activity was observed in **7**, whose twisted conformation provides a stronger solid state emission than the other derivatives. FEG-SEM studies of **7** show that the formation of nanoparticles at 80% f_w in the THF–H_2O mixture are circular in nature, with sizes of 28 to 140 nm. Further, substitution of the donor amine segment on indolo-quinoxaline controls the oxidation potential as well as the HOMO energy level, as measured by CV, which in turn suppresses the HOMO–LUMO energy band gaps; these were found to be in the range of 1.56 to 2.21 eV. The HOMO–LUMO energy values were found to be comparable with those of reported ambipolar materials. The location of electron density in the HOMO and LUMO orbitals obtained by DFT and TD-DFT further verifies the impact of different donor groups and the presence of D–A architectures in the molecules. Thermal studies revealed good thermal stabilities of all the derivatives. Thus, the experimental and theoretical results indicate that modulation of different donor groups on indolo-quinoxaline results in solid state emission with AIE activity and ambipolar properties, which is beneficial for their potential use in various optoelectronic applications.

Experimental section

Chemicals and materials

All starting materials and reagents were purchased from commercial sources (Sigma Aldrich and Alfa Aesar) and were used without any further treatment or purification. The organic solvents were of HPLC and spectroscopic grade, dried and freshly distilled using standard procedures, and handled in moisture-free atmosphere. Column chromatography was carried out using SD Fine silica gel (60 to 120 mesh), eluting with *n*-hexane and chloroform. The progress of the reactions and the purity of the compounds were checked by thin layer chromatography (TLC) on silica gel-coated glass plates, visualized with UV light (365 nm) and in an iodine chamber.

Instrumentation and methods

UV-visible spectra were recorded in 10^{-5} mole L^{-1} solutions in a 1 cm path length quartz cuvette and in neat solid films on a SHIMADZU UV-2401PC at room temperature. The neat solid films of compounds **2–9** were prepared using a spin coater (Holmarc HO-TH-05) at 1000 rpm for 2 min with 6 mg ml^{-1} of sample in chloroform. Quartz substrate was used for the neat solid film studies. The excitation and emission spectra were measured on a SHIMADZU RF-5301PC fluorescence spectrophotometer. The fluorescence quantum yields of derivatives **2–9** were calculated using quinine sulphate in 0.1 M H_2SO_4 (Φ_F = 0.54). AIE UV-visible spectra and emission spectra of 10^{-5} mole L^{-1} THF/H_2O solutions with different percentages of water fraction were studied on a similar instrument. Hydrodynamic particle sizes of **2**, **3**, **5**, **7**, **8** and **9** were obtained by DLS analysis using Zetasizer Ver. 7.12, serial number: MAL1180779. The particle sizes and morphologies of molecule **7** were determined by FEG-SEM analysis using JSM-7600F. Cyclic voltammetry studies were carried out on a computer-controlled PalmSens3 potentiostat/galvanostat. Typically, a three-electrode cell equipped with a glassy carbon working electrode, Ag/AgCl (non-aqueous) reference electrode and platinum (Pt) wire counter electrode was employed. The measurements were carried out with a scan rate of 100 mV s^{-1} at room temperature in anhydrous DCM with tetrabutylammonium hexafluorophosphate solution (0.1 M) as the supporting electrolyte. The potential of the Ag/AgCl reference electrode was calibrated using the ferrocene/ferrocenium redox couple with a known oxidation potential of +5.1 eV. The melting points of the products were determined by the open capillary method. The thermogravimetric analysis (TGA) was performed using a Mettler Toledo instrument (TG) under nitrogen atmosphere. ^1H and ^{13}C NMR spectra were recorded using $CDCl_3$ on a Varian 300 MHz Ultra Shield spectrometer with tetramethylsilane (TMS) as an internal reference at working frequencies of 300 MHz and 75 MHz. Distortionless enhancement by polarization transfer (DEPT-135) experiments were performed with the same NMR spectrometer at a working frequency of

75 MHz to determine the multiplicity of the carbon atom substituted with hydrogens, where signals from $-CH_2$ groups will be negative and signals from –CH and $-CH_3$ groups will be positive. Fourier transform infrared (FT-IR) spectra were recorded on a PerkinElmer Frontier 91579. Mass spectrometric measurements were recorded using MALDI-TOF (Bruker), and elemental analysis was performed on an EA Euro-elemental analysis instrument. DFT and time-dependent density functional theoretical (TDDFT) calculations were performed using the Gaussian 03 software package using B3LYP as the exchange correlation functional at the 6-311G basis set.

Synthetic procedures

2,9-Dibromo-6-ethyl-6*H*-indolo[2,3-*b*]quinoxaline (1). 5-Bromo-1-ethyl-1*H*-indole-2,3-dione as a starting material was prepared according to a reported procedure.[17] Compound **1** was prepared by condensing 5-bromo-1-ethyl-1*H*-indole-2,3-dione (1.8 g, 7 mmol) and 4-bromo-1,2-diaminobenzene (1.32 g, 7 mmol) in acetic acid. The reaction mixture was continuously stirred and refluxed for 3 hours. After completion of the reaction, the reaction mixture was poured in distilled water, filtered and washed with water. The solid thus obtained was then purified by column chromatography using eluent: *n*-hexane : chloroform (95 : 5) to obtain a green solid.

Green solid, yield: 2.03 g (70.88%), m.p.: 205 °C, FT-IR (KBr, ν_{max}/cm^{-1}): 3068, 2977, 2926, 1575, 1464, 1269, 1115, 797, ^{1}H-NMR (300 MHz; $CDCl_3$; TMS): δ (ppm) = 8.50 (1H, d, J = 1.2 Hz), 8.31 (1H, dd, J = 2.1, 1.8 Hz), 7.99 (1H, dd, J = 37.6, 8.9 Hz), 7.80–7.31 (3H, m), 7.26 (1H due to residual $CHCl_3$ in $CDCl_3$, s), 4.47 (2H, q, N–CH_2, J = 6.0 Hz), 1.49 (3H, t, $-CH_3$, J = 7.1 Hz), ^{13}C-NMR (75 MHz; $CDCl_3$): δ (ppm) = 142.53, 133.72, 132.65, 131.58, 130.72, 129.85, 129.44, 128.80, 125.33, 122.77, 120.85, 119.34, 114.01, 111.00, 36.13, 13.59, DEPT-135 (75 MHz; $CDCl_3$): δ (ppm) = 133.94, 132.33, 131.36, 129.96, 128.82, 111.17, 36.59, 13.34, MALDI-TOF: mass calcd for $C_{16}H_{11}Br_2N_3$ [M+]: 405.09; found: 405.79, elemental anal. found: C, 47.42; H, 2.75; Br, 39.43; N, 10.36; calcd for $C_{16}H_{11}Br_2N_3$: C, 47.44; H, 2.74; Br, 39.45; N, 10.37.

General method for the synthesis of 2–9

In a three-necked round bottom flask equipped with a reflux condenser and nitrogen inlet and outlet ports, 2,9-dibromo-6-ethyl-6*H*-indolo[2,3-*b*]quinoxaline (**1**) (0.2 g, 0.5 mmol) and diarylamine/heterocyclic amine (1 mmol) were dissolved in anhydrous toluene (30 ml) under nitrogen atmosphere. The palladium catalyst [$Pd_2(dba)_3$] (5 to 8 mol%), 2-dicyclohexylphoshpino-2′,6′-dimethylbiphenyl (SPhos) (10 to 15 mol%) and sodium-*t*-butoxide (3 mol) were added to the reaction mixture. The reaction mixture was thoroughly stirred under nitrogen atmosphere while the temperature was slowly raised to 110 °C. The reaction mixture was stirred at this temperature for 5 to 12 hours. The reaction mixture was cooled to room temperature and extracted with chloroform (3 × 50 ml) followed by water washing (3 × 50 ml). All the organic layers were combined and dried over anhydrous Na_2SO_4 and evaporated to afford the crude product, which was further purified by silica gel column chromatography (eluent: *n*-hexane:chloroform) to obtain yellow to red solids.

6-Ethyl-N^2,N^2,N^9,N^9-tetraphenyl-6*H*-indolo[2,3-*b*]quinoxaline-2,9-diamine (2). Orange solid, yield: 0.206 g (72.92%), m.p.: 196 °C, FT-IR (KBr, ν_{max}/cm^{-1}): 3049, 2969, 2926, 1587, 1474, 1273, 1115, 747, 686, ^{1}H-NMR (300 MHz; $CDCl_3$; TMS): δ (ppm) = 8.19 (1H, dd, J = 1.8, 1.8 Hz), 7.99 (1H, dd, J = 8.4, 8.7 Hz), 7.73–6.95 (24H, m), 4.47 (2H, q, N–CH_2, J = 6 Hz), 1.49 (3H, t, $-CH_3$, J = 6 Hz), ^{13}C-NMR (75 MHz; $CDCl_3$): δ (ppm) = 149.50, 149.43, 148.05, 146.63, 143.96, 143.26, 142.66, 142.51, 139.76, 136.83, 135.36, 131.10, 131.05, 129.54, 129.41, 129.31, 129.09, 128.44, 127.90, 127.65, 127.41, 127.14, 126.92, 126.85, 126.67, 126.50, 126.39, 126.27, 126.16, 126.04, 125.19, 124.38, 124.31, 124.04, 123.66, 123.37, 122.75, 122.64, 121.47, 120.80, 120.48, 120.09, 117.70, 117.51, 114.57, 109.89, 109.81, 36.17, 13.83, DEPT-135 (75 MHz; $CDCl_3$): δ (ppm) = 129.55, 129.46, 129.22, 128.82, 127.99, 126.60, 125.60, 124.91, 124.07, 123.51, 123.24, 122.82, 122.16, 119.70, 116.58, 109.99, 36.41, 13.94, MALDI-TOF: mass calcd for $C_{40}H_{31}N_5$ [M+]: 581.71; found: 581.54, elemental anal. found: C, 82.58; H, 5.36; N, 12.05; calcd for $C_{40}H_{31}N_5$: C, 82.59; H, 5.37; N, 12.04.

6-Ethyl-N^2,N^9-di(naphthalen-1-yl)-N^2,N^9-diphenyl-6*H*-indolo-[2,3-*b*]quinoxaline-2,9-diamine (3). Orange solid, yield: 0.194 g (57.13%), m.p.: 189 °C, FT-IR (KBr, ν_{max}/cm^{-1}): 3044, 2972, 2932, 1575, 1483, 1259, 1115, 768, ^{1}H-NMR (300 MHz; $CDCl_3$; TMS): δ (ppm) = 8.07–7.84 (8H, m), 7.53–7.27 (16H, m), 7.24–6.89 (7H, (1H extra due to residual $CHCl_3$ in $CDCl_3$), m), 4.42 (2H, q, N–CH_2, J = 6.0 Hz), 1.48 (3H, t, $-CH_3$, J = 7.2 Hz), ^{13}C-NMR (75 MHz; $CDCl_3$): δ (ppm) = 149.50, 149.43, 148.05, 146.63, 143.96, 143.26, 142.66, 142.51, 139.76, 136.83, 135.36, 131.10, 131.05, 129.54, 129.41, 129.31, 129.09, 128.44, 127.90, 127.65, 127.41, 127.14, 126.92, 126.85, 126.67, 126.50, 126.39, 126.27, 126.16, 126.04, 125.19, 124.38, 124.31, 124.04, 123.66, 123.37, 122.75, 122.64, 121.47, 120.80, 120.48, 120.09, 117.70, 117.51, 114.57, 109.89, 109.81, 36.17, 13.83, DEPT-135 (75 MHz; $CDCl_3$): δ (ppm) = 129.54, 129.41, 129.31, 129.09, 128.48, 127.89, 127.65, 127.41, 127.14, 126.96, 126.92, 126.66, 126.49, 126.42, 126.30, 126.16, 126.07, 125.19, 124.37, 124.31, 124.03, 123.66, 123.36, 122.75, 122.64, 121.47, 120.79, 120.48, 117.70, 117.50, 117.43, 114.55, 109.88, 36.17, 14.26, MALDI-TOF: mass calcd for $C_{48}H_{35}N_5$ [M+]: 681.83; found: 681.74, elemental anal. found: C, 84.53; H, 5.18; N, 10.26; calcd for $C_{48}H_{35}N_5$: C, 84.55; H, 5.17; N, 10.27.

6-Ethyl-N^2,N^2,N^9,N^9-tetrakis(4-methoxyphenyl)-6*H*-indolo-[2,3-*b*]quinoxaline-2,9-diamine (4). Red solid, yield: 0.135 g (43.4%), m.p.: 210 °C, FT-IR (KBr, ν_{max}/cm^{-1}): 3059, 2926, 2840, 1483, 1239, 1115, 1033, 819, ^{1}H-NMR (300 MHz; $CDCl_3$; TMS): δ (ppm) = 8.05 (1H, dd, J = 1.8, 1.8 Hz), 7.90 (1H, dd, J = 9.3, 9.0 Hz), 7.52–6.77 (21H (1H extra due to residual $CHCl_3$ in $CDCl_3$), m), 4.45 (2H, q, N–CH_2, J = 7.2 Hz), 3.80 (12H, s, $-OCH_3$), 1.47 (3H, t, $-CH_3$, J = 6.2 Hz), ^{13}C-NMR (75 MHz; $CDCl_3$): δ (ppm) = 156.67, 156.28, 155.16, 149.50, 147.07, 142.93, 142.78, 142.21, 142.15, 140.76, 140.39, 140.24, 138.57, 136.40, 127.54, 127.35, 126.94, 126.50, 125.16, 124.78, 120.82, 120.17, 117.22, 116.89, 115.99, 114.97, 114.93, 112.93, 109.75, 109.66, 55.44, 36.14, 13.64, DEPT-

135 (75 MHz; $CDCl_3$): δ (ppm) = 131.18, 129.31, 127.54, 127.34, 126.94, 126.50, 125.16, 124.78, 120.97, 117.21, 116.88, 115.97, 114.96, 114.92, 114.72, 112.91, 109.75, 109.67, 55.52, 36.14, 13.63, MALDI-TOF: mass calcd for $C_{44}H_{39}N_5O_4$ [M+]: 701.81; found: 701.53, elemental anal. found: C, 75.29; H, 5.62; N, 9.97; O, 9.11; calcd for $C_{44}H_{39}N_5O_4$: C, 75.30; H, 5.60; N, 9.98; O, 9.12.

6-Ethyl-*N*^{2},*N*^{9}-bis(4-nitrophenyl)-*N*^{2},*N*^{9}-diphenyl-6*H*-indolo-[2,3-*b*]quinoxaline-2,9-diamine (5). Red solid, yield: 0.176 g (51.6%); m.p.: 203 °C, FT-IR (KBr, ν_{max}/cm^{-1}): 3049, 2977, 2905, 1596, 1473, 1296, 1094, 675, ^{1}H-NMR (300 MHz; $CDCl_3$; TMS): δ (ppm) = 8.24 (1H, dd, J = 1.8, 1.8 Hz), 8.12–7.91 (6H, m), 7.59–6.91 (18H (1H extra due to residual $CHCl_3$ in $CDCl_3$), m), 4.54 (2H, q, N–CH_2, J = 7.2 Hz), 1.54 (3H, t, –CH_3, J = 6.2 Hz), ^{13}C-NMR (75 MHz; $CDCl_3$): δ (ppm) = 153.88, 153.82, 153.12, 153.02, 145.79, 145.75, 145.67, 145.63, 143.82, 141.84, 140.87, 139.99, 139.30, 139.25, 138.72, 130.49, 130.24, 130.19, 130.13, 130.04, 129.08, 127.76, 127.05, 126.88, 126.32, 126.18, 125.76, 125.56, 125.49, 124.40, 124.11, 121.55, 121.41, 120.56, 120.29, 119.23, 117.53, 36.26, 13.55, DEPT-135 (75 MHz; $CDCl_3$): δ (ppm) = 130.49, 130.24, 130.19, 130.13, 130.03, 129.06, 127.76, 127.04, 126.87, 126.33, 126.18, 125.75, 125.49, 124.40, 124.10, 121.55, 121.51, 121.41, 120.28, 119.22, 117.51, 110.88, 110.81, 36.39, 13.76, MALDI-TOF: mass calcd for $C_{40}H_{29}N_7O_4$ [M+]: 671.70; found: 671.07, elemental anal. found: C, 71.51; H, 4.34; N, 14.62; O, 9.55; calcd for $C_{40}H_{29}N_7O_4$: C, 71.52; H, 4.35; N, 14.60; O, 9.53.

6-Ethyl-*N*^{2},*N*^{9}-diphenyl-*N*^{2},*N*^{9}-bis(4-((*E*)-phenyldiazenyl)phenyl)-6*H*-indolo[2,3-*b*]quinoxaline-2,9-diamine (6). Red solid, yield: 0.175 g (45.2%), m.p.: 214 °C, FT-IR (KBr, ν_{max}/cm^{-1}): 3059, 2977, 2926, 1586, 1442, 1217, 1115, 747, ^{1}H-NMR (300 MHz; $CDCl_3$; TMS): δ (ppm) = 8.30 (1H, dd, J = 2.1, 2.1 Hz), 8.29–7.73 (12H, m), 7.51–7.12 (21H, m), 4.48 (2H, q, N–CH_2, J = 7.05 Hz), 1.50 (3H, t, –CH_3, J = 7.2 Hz), ^{13}C-NMR (75 MHz; $CDCl_3$): δ (ppm) = 152.99, 152.87, 151.08, 149.96, 148.24, 147.81, 147.21, 146.92, 146.65, 146.03, 142.04, 140.66, 140.60, 136.38, 130.48, 130.10, 129.94, 129.84, 129.59, 129.52, 129.05, 128.99, 126.37, 125.13, 125.05, 124.36, 123.95, 123.79, 123.65, 122.64, 122.58, 122.49, 120.97, 120.74, 120.62, 119.06, 110.32, 36.38, 14.12, DEPT-135 (75 MHz; $CDCl_3$): δ (ppm) = 130.48, 130.10, 129.93, 129.84, 129.59, 129.52, 129.05, 128.99, 126.37, 126.05, 125.13, 125.05, 124.76, 124.35, 123.95, 123.78, 123.64, 122.63, 122.48, 121.97, 120.83, 120.73, 120.61, 119.04, 110.32, 36.25, 13.98, MALDI-TOF: mass calcd for $C_{52}H_{39}N_9$ [M+]: 789.93; found: 789.45, elemental anal. found: C, 79.06; H, 4.97; N, 15.98; calcd for $C_{52}H_{39}N_9$: C, 79.07; H, 4.98; N, 15.96.

2,9-Di(9*H*-carbazol-9-yl)-6-ethyl-6*H*-indolo[2,3-*b*]quinoxaline (7). Yellow solid, yield: 0.207 g (73.1%), m.p.: 198 °C, FT-IR (KBr, ν_{max}/cm^{-1}): 3049, 2926, 2844, 1586, 1483, 1269, 1115, 686, ^{1}H-NMR (300 MHz; $CDCl_3$; TMS): δ (ppm) = 8.68 (1H, dd, J = 1.5, 1.8 Hz), 8.48–8.34 (2H, m), 8.16–8.13 (4H, m), 7.87–7.21 (16H (1H extra due to residual $CHCl_3$ in $CDCl_3$), m), 4.62 (2H, q, N–CH_2, J = 7.2 Hz), 1.62 (3H, t, –CH_3, J = 7.5 Hz), ^{13}C-NMR (75 MHz; $CDCl_3$): δ (ppm) = 145.80, 143.03, 142.88, 141.55, 141.43, 140.79, 140.62, 140.17, 139.86, 139.75, 138.23, 135.48, 131.06, 130.96, 130.54, 130.30, 129.32, 128.24, 126.49, 126.13, 126.10, 125.98, 125.10, 124.61, 123.75, 123.60, 123.29, 121.99, 121.81, 120.73, 120.50, 120.45, 120.35, 120.31, 119.97, 110.81, 110.60, 109.78, 109.63, 36.71, 13.93, DEPT-135 (75 MHz; $CDCl_3$): δ (ppm) = 134.23, 133.69, 133.27, 131.21, 130.42, 130.13, 128.77, 127.64, 127.59, 127.11, 126.95, 126.88, 126.81, 126.75, 125.37, 124.07, 123.99, 123.26, 123.16, 122.49, 122.44, 121.17, 120.65, 120.41, 117.87, 116.03, 115.30, 113.29, 111.72, 111.46, 110.85, 36.47, 13.79, MALDI-TOF: mass calcd for $C_{40}H_{27}N_5$ [M+]: 577.68; found: 577.44, elemental anal. found: C, 83.16; H, 4.70; N, 12.14; calcd for $C_{40}H_{27}N_5$: C, 83.17; H, 4.71; N, 12.12.

10,10′-(6-Ethyl-6*H*-indolo[2,3-*b*]quinoxaline-2,9-diyl)bis(10*H*-phenoxazine) (8). Red solid, yield: 0.132 g (44.1%), m.p.: 184 °C, FT-IR (KBr, ν_{max}/cm^{-1}): 3060, 2977, 2926, 1586, 1473, 1269, 736, ^{1}H-NMR (300 MHz; $CDCl_3$; TMS): δ (ppm) = 8.56 (1H, s), 8.34–8.29 (2H, m), 8.01 (1H, d, J = 2.4 Hz), 7.78–7.71 (3H, m), 7.25–6.80 (12H (1H extra due to residual $CHCl_3$ in $CDCl_3$), m), 6.51–6.24 (4H, m), 4.63 (2H, q, N–CH_2, J = 7.2 Hz), 1.61 (3H, t, –CH_3, J = 6.6 Hz), ^{13}C-NMR (75 MHz; $CDCl_3$): δ (ppm) = 146.05, 144.76, 143.85, 143.20, 141.91, 140.68, 139.41, 134.64, 133.40, 131.22, 129.91, 128.93, 128.01, 127.36, 126.06, 124.49, 124.24, 122.95, 122.65, 122.00, 121.01, 120.08, 117.59, 115.94, 111.86, 111.52, 110.62, 36.75, 14.02, DEPT-135 (75 MHz; $CDCl_3$): δ (ppm) = 134.25, 133.74, 131.21, 130.33, 128.80, 127.67, 127.13, 126.98, 126.84, 126.78, 125.94, 124.57, 124.08, 123.19, 122.51, 122.47, 121.94, 120.65, 117.91, 116.07, 111.73, 111.57, 36.77, 14.05, MALDI-TOF: mass calcd for $C_{40}H_{27}N_5O_2$ [M+]: 609.67; found: 609.31, elemental anal. found: C, 78.81; H, 4.45; N, 11.48; O, 5.24; calcd for $C_{40}H_{27}N_5O_2$: C, 78.80; H, 4.46; N, 11.49; O, 5.25.

10,10′-(6-Ethyl-6*H*-indolo[2,3-*b*]quinoxaline-2,9-diyl)bis(10*H*-phenothiazine) (9). Red solid, yield: 0.135 g (43.0%), m.p.: 192 °C, FT-IR (KBr, ν_{max}/cm^{-1}): 3059, 2977, 2916, 1575, 1453, 1227, 1115, 737, ^{1}H-NMR (300 MHz; $CDCl_3$; TMS): δ (ppm) = 8.58–8.56 (1H, m), 8.33–8.28 (1H, m), 8.01–7.62 (3H, m), 7.36–6.48 (14H, m), 6.31–6.10 (3H, m), 4.63 (2H, q, N–CH_2, J = 6.9 Hz), 1.60 (3H, t, –CH_3, J = 6.8 Hz), ^{13}C-NMR (75 MHz; $CDCl_3$): δ (ppm) = 144.63, 144.59, 143.99, 143.90, 143.40, 143.14, 143.03, 142.15, 141.22, 140.33, 139.79, 139.48, 138.83, 134.30, 134.22, 131.22, 130.13, 128.78, 127.64, 127.59, 127.11, 126.95, 126.82, 126.75, 125.99, 124.06, 123.99, 123.26, 123.16, 122.49, 120.63, 120.18, 117.88, 116.02, 113.44, 113.30, 111.71, 110.86, 36.73, 13.62, DEPT-135 (75 MHz; $CDCl_3$): δ (ppm) = 134.23, 133.69, 133.27, 131.21, 130.13, 128.77, 127.64, 127.59, 127.11, 126.95, 126.88, 126.81, 126.75, 126.29, 125.92, 125.37, 124.07, 123.99, 117.87, 116.03, 115.30, 113.29, 36.73, 13.63, MALDI-TOF: mass calcd for $C_{40}H_{27}N_5S_2$ [M+]: 641.81; found: 641.13, elemental anal. found: C, 74.84; H, 4.23; N, 10.90; S, 9.98; calcd for $C_{40}H_{27}N_5S_2$: C, 74.86; H, 4.24; N, 10.91; S, 9.99.

Preparation of nanoaggregates

10^{-4} M concentrations of stock THF solutions were prepared. Aliquots of the stock solution were transferred to 5 ml volumetric flasks. After appropriate addition of THF, water was added dropwise under vigorous stirring to furnish 10^{-5} M solutions with different water contents (0 to 90 vol%). The

photophysical measurements of the resulting solutions were then performed immediately.

Conflicts of interest

There are no conflicts to declare.

Acknowledgements

The authors are greatly thankful to Micro-Analytical Laboratory, Department of Chemistry, and University of Mumbai for providing instrumental facilities, National NMR centre and Department of Chemistry, TIFR-Mumbai for providing MALDI-TOF and SAIF-IIT Bombay for enabling FEG-SEM characterisation. P. S. Singh is thankful to University Grant Commission, India for Research Fellowship.

References

1 (*a*) J. Harmenberg, W. J. A. N. Bergman, S. Akerfeldt and L. Lundlad, *Antimicrob. Agents Chemother.*, 1988, **32**, 1720; (*b*) J. Hirata, S. Araya, K. K. Nakaike and T. Ishida, *Chem. Pharm. Bull.*, 2001, **49**, 44; (*c*) K. Manna and Y. K. Agrawal, *Bioorg. Med. Chem. Lett.*, 2009, **19**, 2688.

2 (*a*) K. R. J. Thomas and P. Tyagi, *J. Org. Chem.*, 2010, **75**, 8100; (*b*) P. Tyagi, A. Venkateswararao and K. R. J. Thomas, *J. Org. Chem.*, 2011, **76**, 4571; (*c*) T.-H. Su, C.-H. Fan, Y.-H. Yang, L.-C. Hsu and C.-H. Chemg, *J. Mater. Chem. C*, 2013, **1**, 5084; (*d*) A. Venkateswarao, P. Tyagi, K. R. J. Thomas and P. W. Chen, *et al.*, *Tetrahedron*, 2014, **70**, 6318; (*e*) A.-J. Payne, J. S. J. McCahill and G. C. Welch, *Dyes Pigm.*, 2015, **12**, 3139; (*f*) A. M. Shaikh, B. K. Sharma and R. M. Kamble, *Can. Chem. Trans.*, 2015, **3**, 158; (*g*) B. K. Sharma, A. M. Shaikh, S. Chacko and R. M. Kamble, *J. Chem. Sci.*, 2017, **129**, 483; (*h*) R. M. Kamble, B. K. Sharma, A. M. Shaikh and S. Chacko, *ChemistrySelect*, 2018, **3**, 6907.

3 B. Przyjazna, Z. Kucybała and J. P. Czkowski, *Polymer*, 2004, **45**, 2559.

4 (*a*) J. Waluk and S. J. Komorowski, *Chem. Phys. Lett.*, 1987, **133**, 368; (*b*) J. Waluk and E. W. Thulstrup, *Spectrochim. Acta*, 1988, **44**, 1335.

5 (*a*) A. Kraft, A. C. Grimsdale and A. B. Holmes, *Angew. Chem., Int. Ed.*, 1998, **37**, 402; (*b*) A. P. Kulkarni, C. J. Tonzola, A. Babel and S. A. Jenekhe, *Chem. Mater.*, 2004, **16**, 4556.

6 (*a*) B. L. Lee and T. Yamamoto, *Macromolecules*, 1999, **32**, 1375; (*b*) S. A. Jenekhe, L. Lu and M. M. Alam, *Macromolecules*, 2001, **34**, 7315; (*c*) S. Tao, L. Li, J. Yu, Y. Jiang, Y. Zhou, C.-S. Lee, S.-T. Lee, X. Zhang and O. Kwon, *Chem. Mater.*, 2009, **21**, 1284; (*d*) A. Mishra, M. K. R. Fischer and P. Beauerle, *Angew. Chem., Int. Ed.*, 2009, **48**, 2474.

7 (*a*) D. W. Chang, S. J. Ko, J. Y. Kim, L. Dai and J. B. Baek, *Synth. Met.*, 2012, **162**, 1169; (*b*) A. M. Shaikh, B. K. Sharma and R. M. Kamble, *J. Chem. Sci.*, 2015, **9**, 1571; (*c*) A. M. Shaikh, B. K. Sharma, S. Chacko and R. M. Kamble, *RSC Adv.*, 2016, **6**, 60084; (*d*) P. S. Singh, S. Chacko and R. M. Kamble, *New J. Chem.*, 2019, **43**, 6973; (*e*) D. N. Kanekar, S. Chacko and R. M. Kamble, *Dyes Pigm.*, 2019, **167**, 36; (*f*) S. S. Mahadik, S. Chacko and R. M. Kamble, *ChemistrySelect*, 2019, **4**, 10021; (*g*) A. M. Shaikh, B. K. Sharma and R. M. Kamble, *Chem. Heterocycl. Compd.*, 2016, **52**, 110.

8 (*a*) Z. Wang, X. Song, L. Ma, Y. Feng, C. Gu, X. Zhang, P. Lu and Y. Mab, *New J. Chem.*, 2013, **37**, 2440; (*b*) A. M. Shaikh, B. K. Sharma, S. Chacko and R. M. Kamble, *RSC Adv.*, 2016, **6**, 94218; (*c*) A. M. Shaikh, B. K. Sharma, S. Chacko and R. M. Kamble, *New J. Chem.*, 2017, **41**, 628.

9 (*a*) S. A. Jenekhe and J. A. Osaheni, *Science*, 1994, **265**, 765; (*b*) B. K. An, S. K. Kwon, S. D. Jung and S. Y. Park, *J. Am. Chem. Soc.*, 2002, **124**, 14410; (*c*) S. Jayanty and T. P. Radhakrishnan, *Chem. – Eur. J.*, 2004, **10**, 791; (*d*) Z. R. Grabowski, K. Rotkiewicz and W. Rettig, *Chem. Rev.*, 2003, **103**, 3899.

10 (*a*) C. W. Tang and S. A. VanSlyke, *Appl. Phys. Lett.*, 1987, **51**, 913; (*b*) R. H. Friend, R. W. Gymer, A. B. Holmes, J. H. Burroughes, R. N. Marks and C. Taliani, *et al.*, *Nature*, 1999, **397**, 121.

11 J. Luo, Z. Xie, J. W. Y. Lam, L. Cheng, H. Chen, C. Qiu, H. S. Kwok, X. Zhan, Y. Liu, D. Zhu and B. Z. Tang, *Chem. Commun.*, 2001, 1740.

12 W. Z. Yuan, P. Lu, S. Chen, J. W. Y. Lam, Z. Wang, Y. Liu, H. S. Kwok, Y. Ma and B. Z. Tang, *Adv. Mater.*, 2010, **22**, 2159.

13 (*a*) K. Zhou, H. Dong, H. L. Zhang and W. Hu, *Phys. Chem. Chem. Phys.*, 2014, **16**, 22448; (*b*) A. M. Shaikh, S. Chacko and R. M. Kamble, *ChemistrySelect*, 2017, **2**, 7620.

14 (*a*) Y. Sakamoto, T. Suzuki, M. Kobayashi, Y. Gao, Y. Fukai and Y. Inoue, *et al.*, *J. Am. Chem. Soc.*, 2004, **126**, 8138; (*b*) Z. Liang, Q. Tang, J. Xu and Q. Miao, *Adv. Mater.*, 2011, **23**, 1535.

15 (*a*) L. Chen, Y. Jiang, H. Nie, R. Hu, H. S. Kwok and F. Huang, *et al.*, *ACS Appl. Mater. Interfaces*, 2014, **6**, 17215; (*b*) Y. Shirota, M. Kinoshita, T. Noda, K. Okumoto and T. A. Ohara, *J. Am. Chem. Soc.*, 2000, **122**, 11021.

16 (*a*) A. S. Guran and S. L. Buchwald, *J. Am. Chem. Soc.*, 1994, **116**, 7901; (*b*) F. Paul, J. Patt and J. F. Hartwig, *J. Am. Chem. Soc.*, 1994, **116**, 5969.

17 (*a*) A. Beauchard, Y. Ferandin, S. Frère, O. Lozach, M. Blairvacq, L. Meijer, V. Thiery and T. Besson, *Bioorg. Med. Chem.*, 2006, **14**, 6434; (*b*) A. Tarek, A. B. J. Fayzah and A. W. Omima, *Eur. J. Med. Chem.*, 2010, **45**, 4578.

18 C. Reichardt, *Chem. Rev.*, 1994, **94**, 2319.

19 S. Xue, W. Liu, X. Qiu, Y. Gao and W. Yang, *J. Phys. Chem. C*, 2014, **118**, 18668.

20 J. Guo, X.-L. Li, H. Nie, W. Luo, R. Hu and A. Qin, *et al.*, *Chem. Mater.*, 2017, **29**, 3623.

21 Z. Wang, Z. Peng, K. Huang, P. Lu and Y. Wang, *J. Mater. Chem. C*, 2019, **7**, 6706.

22 (*a*) W. Rettig, *Angew. Chem., Int. Ed. Engl.*, 1986, **25**, 971; (*b*) J. F. Letard, R. Lapouyade and W. Rettig, *J. Am. Chem. Soc.*, 1993, **115**, 2441.

23 K. M. Franziska and J. J. M. Thomas, *Sci. China: Chem.*, 2018, **61**, 909.

24 M. Sauer, J. Hofkens and J. Enderlein, *Handbook of Fluorescence Spectroscopy and Imaging*, WILEY-VCH Verlag GmbH & Co. KGaA, Weinheim, 2011.

25 (*a*) J. Daub, R. Engl, J. Kurzawa, S. E. Miller, S. Schneider, A. Stockmann and M. R. Wasielewski, *J. Phys. Chem. A*, 2001, **105**, 5655; (*b*) P. A. Kulkarni, P. T. Wu, T. W. Kwonand and S. A. Jenekhe, *J. Phys. Chem. B*, 2005, **109**, 19584; (*c*) D. W. Cho, M. Fujitsuka, A. Sugimoto, U. C. Yoon, P. S. Mariano and T. Majima, *J. Phys. Chem. B*, 2006, **110**, 11062.

26 S.-S. Sun and C. E. Bonner, *Organic Photovoltaics: Mechanisms, Materials, and Device*, ed. S.-S. Sun and N. S. Sariciftci, Taylor and Francis, USA, 1st edn, 2005, ch. 8, pp. 183–216.

27 Z. Ning, Z. Chen, Q. Zhang, Y. Yan, S. Qian, Y. Cao and H. Tian, *Adv. Funct. Mater.*, 2007, **17**, 3799.

28 (*a*) Z. Li, Y. Dong, B. Mi, Y. Tang, M. Haussler, H. Tong and Y. Dong, *et al.*, *J. Phys. Chem. B*, 2005, **109**, 10061; (*b*) S. Xue, W. Liu, X. Qiu, Y. Gao and W. Yang, *J. Phys. Chem. C*, 2014, **118**, 18668.

29 Y. Zhan and H. Hu, *Dyes Pigm.*, 2019, **167**, 127.

30 (*a*) R. H. Friend, R. W. Gymer, A. B. Holms, J. H. Burroughes, R. N. Marks and C. Taliani, *et al.*, *Nature*, 1999, **397**, 121; (*b*) Y. Liu, X. T. Tao, F. Z. Wang, X. N. Dang, D. C. Zou and Y. Ren, *et al.*, *J. Phys. Chem. C*, 2008, **112**, 3975.

31 H. Kasai, H. S. Nalwa, H. Oikawa, S. Okada, H. Matsuda and N. Minami, *et al.*, *Jpn. J. Appl. Phys.*, 1992, **31**, L1132.

32 (*a*) H. Auweter, H. Haberkorn, W. Heckmann, D. Horn, E. Luddecke, J. Rieger and H. Weiss, *Angew. Chem., Int. Ed.*, 1999, **38**, 2188; (*b*) J. Mei, J. Wang, J. Z. Sun, H. Zhao, W. Yuan, C. Deng and S. Chen, *et al.*, *Chem. Sci.*, 2012, **3**, 549.

33 J. Mei, N. L. C. Leung, R. T. K. Kwok, J. W. Y. Lam and B. Z. Tang, *Chem. Rev.*, 2015, **115**, 11718.

34 (*a*) Y. Hong, J. W. Y. Lam and B. Z. Tang, *Chem. Soc. Rev.*, 2011, **40**, 5361; (*b*) X. Luo, J. Li, C. Li, L. Heng, Y. Q. Dong and Z. Liu, *et al.*, *Adv. Mater.*, 2011, **23**, 3261; (*c*) W. Liu, S. Ying, Q. Zhang, S. Ye, R. Guo and D. Ma, *et al.*, *Dyes Pigm.*, 2018, **158**, 204.

35 C. Wu, Z. Wu, B. Wang, X. Li, N. Zhao and J. Hu, *et al.*, *ACS Appl. Mater. Interfaces*, 2017, **9**, 32946.

36 J. Armand, L. Boulares, C. Bellec and J. Pinson, *Can. J. Chem.*, 1982, **60**, 2797.

37 (*a*) K. R. J. Thomas, J. T. Lin, Y.-T. Tao and C.-H. Chuen, *Chem. Mater.*, 2005, **17**, 1860; (*b*) K. R. J. Thomas, J. T. Lin, Y.-T. Tao and C.-H. Chuen, *Chem. Mater.*, 2002, **14**, 2796.

38 (*a*) F. C. Franco and A. A. B. Padama, *Polymer*, 2016, **97**, 55; (*b*) O. Kwon, S. Barlow, S. A. Odom, L. Beverina, N. J. Thompson and E. Zojer, *et al.*, *J. Phys. Chem. A*, 2005, **109**, 9346.

39 A. J. Kronemeijer, D. I. James, H. Sirringhaus, I. McCullocha and R. S. Ashraf, *Chem. Commun.*, 2012, **48**, 3939.

40 (*a*) B. A. Jones, A. Facchetti, M. R. Wasielewski and T. J. Marks, *J. Am. Chem. Soc.*, 2007, **129**, 15259; (*b*) D. N. Kanekar, S. Chacko and R. M. Kamble, *ChemistrySelect*, 2018, **3**, 4114.

41 Z. Liang, Q. Tang, R. Mao, D. Liu, J. Xu and Q. Miao, *Adv. Mater.*, 2011, **23**, 5514.

42 H. Xia, D. Q. Liu, X. M. Xu and Q. Miao, *Chem. Commun.*, 2013, **49**, 4301.

43 Y. Li, B. Sun, P. Sonar and S. P. Singh, *Org. Electron.*, 2012, **13**, 1606.

44 B. C. Thompson and J. M. J. Frechet, *Angew. Chem., Int. Ed.*, 2008, **47**, 58.

45 R. Kroon, M. Lenes, J. C. Hummelen, P. W. M. Blom and B. D. Boer, *Polym. Rev.*, 2008, **48**, 531.

46 L. Wang, X. Zhang, H. Tian, Y. Lu, Y. Geng and F. Wang, *Chem. Commun.*, 2013, **49**, 11272.

47 M. X. Yu, J. P. Duan, C. H. Lin, C. H. Cheng and Y. T. Tao, *Chem. Mater.*, 2002, **14**, 3958.

48 M. J. Frisch, G. W. Trucks, H. B. Schlegel, G. E. Scuseria, M. A. Robb, J. R. Cheeseman, J. A. Montgomery Jr, T. Vreven, K. N. Kudin, J. C. Burant, J. M. Millam, S. S. Iyengar, J. Tomasi, V. Barone, B. Mennucci, M. Cossi, G. Scalmani, N. Rega, G. A. Petersson, H. Nakatsuji, M. Hada, M. Ehara, K. Toyota, R. Fukuda, J. Hasegawa, M. Ishida, T. Nakajima, Y. Honda, O. Kitao, H. Nakai, M. Klene, X. Li, J. E. Knox, H. P. Hratchian, J. B. Cross, V. Bakken, C. Adamo, J. Jaramillo, R. Gomperts, R. E. Stratmann, O. Yazyev, A. J. Austin, R. Cammi, C. Pomelli, J. W. Ochterski, P. Y. Ayala, K. Morokuma, G. A. Voth, P. Salvador, J. J. Dannenberg, V. G. Zakrzewski, S. Dapprich, A. D. Daniels, M. C. Strain, O. Farkas, D. K. Malick, A. D. Rabuck, K. Raghavachari, J. B. Foresman, J. V. Ortiz, Q. Cui, A. G. Baboul, S. Clifford, J. Cioslowski, B. B. Stefanov, G. Liu, A. Liashenko, P. Piskorz, I. Komaromi, R. L. Martin, D. J. Fox, T. Keith, M. A. Al-Laham, C. Y. Peng, A. Nanayakkara, M. Challacombe, P. M. W. Gill, B. Johnson, W. Chen, M. W. Wong, C. Gonzalez and J. A. Pople, *Gaussian, 03, Revision C.02*, Gaussian, Inc., Wallingford CT, 2004.

49 Y. Zhu, A. P. Kulkani, P.-T. Wu and S. A. Jenekhe, *Chem. Mater.*, 2008, **20**, 4200.

50 (*a*) S. Bay and T. Müller, *Z. Naturforsch. B*, 2014, **69**, 541; (*b*) A. P. Kulkarni, P. Wu, T. W. Kwon and S. A. Jenekhe, *J. Phys. Chem. B*, 2005, **109**, 19584.

51 (*a*) A. Elangovan, K.-M. Kao, S.-W. Yang, Y.-L. Chen, T.-I. Ho and Y. O. J. Su, *J. Org. Chem.*, 2005, **70**, 4460; (*b*) J. A. Marsden, J. J. Miller, L. D. Shirtcliff and M. M. J. Haley, *J. Am. Chem. Soc.*, 2005, **127**, 2464.

